

1 **Effects of Urban Land Expansion on the Regional**
2 **Meteorology and Air Quality of Eastern China**

3

4 **W. Tao¹, J. Liu^{1*}, G. A. Ban-Weiss², D. A. Hauglustaine³, L. Zhang⁴, Q. Zhang⁵, Y.**
5 **Cheng⁶, Y. Yu⁷, and S. Tao¹**

6

7 [1]{Laboratory for Earth Surface Processes, College of Urban and Environmental Sciences,
8 Peking University, Beijing 100871, China}

9 [2]{Sonny Astani Department of Civil and Environmental Engineering, University of
10 Southern California, U.S.A.}

11 [3]{Laboratoire des Sciences du Climat et de l'Environnement, UMR 8212, CEA-CNRS-
12 UVSQ, Gif-sur-Yvette, France}

13 [4]{Laboratory for Climate and Ocean-Atmosphere Sciences, Department of Atmospheric
14 and Oceanic Sciences, School of Physics, Peking University, Beijing 100871, China}

15 [5]{Center for Earth System Science, Tsinghua University, Beijing 100084, China}

16 [6]{Chinese Academy of Meteorological Sciences, Beijing, China}

17 [7]{Nanjing Municipal Environmental Monitoring Centre, Nanjing, Jiangsu 210013, China}

18

19

20 Correspondence to: J. Liu (E-mail: jfliu@pku.edu.cn)

21

1 **Abstract**

2 Rapid urbanization throughout Eastern China is imposing an irreversible effect on local
3 climate and air quality. In this paper, we examine the response of a range of meteorological
4 and air quality indicators to urbanization. Our study uses the Weather Research and
5 Forecasting model coupled with Chemistry (WRF/Chem) to simulate the climate and air
6 quality impacts of four hypothetical urbanization scenarios with fixed surface pollutant
7 emissions during the month of July from 2008 to 2012. An improved integrated process rate
8 (IPR) analysis scheme is implemented in WRF/Chem to investigate the mechanisms behind
9 the forcing–response relationship at the process level. For all years, as urban land area
10 expands, concentrations of CO, elemental carbon (EC), and particulate matter with
11 aerodynamic diameter less than 2.5 microns (PM_{2.5}) tend to decrease near the surface (below
12 ~500 m), but increase at higher altitudes (1–3 km), resulting in a reduced vertical
13 concentration gradient. On the other hand, the O₃ burden averaged over all newly urbanized
14 grid cells consistently increases from the surface to a height of about 4 km. Sensitivity tests
15 show that the responses of pollutant concentrations to the spatial extent of urbanization are
16 nearly linear near the surface, but nonlinear at higher altitudes. Over eastern China, each 10%
17 increase in nearby urban land coverage on average leads to a decrease of approximately 2% in
18 surface concentrations for CO, EC, and PM_{2.5}, while for O₃ an increase of about 1% is
19 simulated. At 800 hPa, pollutants' concentrations tend to increase even more rapidly with
20 increase in nearby urban land coverage. This indicates that as large tracts of new urban land
21 emerge, the influence of urban expansion on meteorology and air pollution would be
22 significantly amplified. IPR analysis reveals the contribution of individual atmospheric
23 processes to pollutants' concentration changes. It indicates that, for primary pollutants, the
24 enhanced sink (source) caused by turbulent mixing and vertical advection in the lower (upper)
25 atmosphere could be a key factor in changes to simulated vertical profiles. The evolution of
26 secondary pollutants is further influenced by the upward relocation of precursors that impact
27 gas phase chemistry for O₃ and aerosol processes for PM_{2.5}. Our study indicates that dense
28 urbanization has a moderate dilution effect on surface primary airborne contaminants, but
29 may intensify severe haze and ozone pollution if local emissions are not well controlled.

30 **Keywords:** Urbanization, Air pollution, Process analysis, Linearity, Aerosol, Ozone

1 **1 Introduction**

2 Urbanization refers to the growth of urban populations and the vast expansion of urban areas.
3 According to the 2011 Revision of the United Nations (UN) World Urbanization Prospects,
4 the global proportion of the population living in urban areas is likely to increase to 68%
5 (about 6.2 billion) by 2050, and the urban population in less developed regions will almost
6 double from 2.7 billion in 2011 to 5.1 billion in 2050 (Heilig, 2012). The environmental side-
7 effects of urbanization, such as inadvertent climate modification (Changnon, 1992) and air
8 quality degradation (Mage et al., 1996), remain an important research topic with societal
9 relevance.

10 The radiative, thermal, hydrologic, and aerodynamic properties of urban land surfaces are
11 distinct from those of natural surfaces (e.g., forests, grassland), resulting in unique exchange
12 processes of energy, moisture, and momentum with the ambient atmosphere and thus distinct
13 climatic conditions in urban areas (Oke, 1987). The features of urban climate (e.g. urban heat
14 island (UHI), wind profiles in the urban canopy layer) have been extensively observed,
15 modeled and comprehensively reviewed (e.g. Arnfield, 2003; Kanda, 2007; Souch and
16 Grimmond, 2006). The urban climate is characterized by multiple scales (Britter and Hanna,
17 2003; Fisher et al., 2006; Oke, 2006), e.g. flows in the roughness sublayer at micro-scale are
18 not subject to Monin–Obukhov similarity relationships, whereas upper flows in the inertial
19 layer are in equilibrium with the underlying surface, and can be described by meso-scale
20 dynamics. Another feature of urban climatology is, heterogeneity, namely the high non-
21 uniformities of roughness elements (e.g. impervious road, green belt, etc.) in urban areas
22 make it rather complicated to generalize the urban flow details from one landscape to another
23 (Fernando et al., 2001). Factors as anthropogenic heat (Fan and Sailor, 2005), chemistry–
24 climate feedbacks (Rosenfeld, 2000), and topography could alter the characteristics of urban
25 climatic conditions, and the intensity of background wind speed or land-sea breezes could
26 impact the structure of urban boundary layer (Fisher et al., 2006; Rotach et al., 2002) and the
27 ventilation conditions as well (Ryu et al., 2013; Yoshikado and Tsuchida, 1996).

28 Up to now, a number of urban canopy schemes have been developed (e.g.,Coceal and Belcher,
29 2004; Di Sabatino et al., 2008; Harman et al., 2004; Luhar et al., 2014; Solazzo et al., 2010;
30 Trusilova et al., 2013; Wang et al., 2011). Among which four schemes with different
31 complexities have been implemented in the mesoscale meteorological model (WRF) to
32 account for the effects of urban areas on urban climate, namely Bulk (BULK, Liu et al., 2006),

1 Single-layer Urban Canopy Model (SLUCM, Kusaka and Kimura, 2004), Building Effect
2 Parameterization (BEP, Martilli et al., 2002), and Building Energy Model (coupled to BEP,
3 denoted as BEP+BEM, Salamanca et al., 2010). The BULK scheme parameterizes the urban
4 surface with greater heat capacity, thermal conductivity, roughness length, and lower albedo
5 than those of natural land surfaces, and has been successfully employed in real-time weather
6 forecasts (Liu et al., 2006). It could capture the features of urban synoptic conditions (Liao et
7 al., 2014), and is being widely used for real-time meso-scale weather forecasting over urban
8 areas (Salamanca et al., 2011). The last three schemes represent the urban geometry as street
9 canyons with urban surfaces (i.e., walls, roofs, and roads), and the coupled WRF-SLUCM
10 model reportedly has the ability to capture the UHI features in some megacities (Cui and de
11 Foy, 2012; Lin et al., 2011; Miao et al., 2009). However, application of these urban canopy
12 schemes requires specifying a vast number of urban canopy parameters and initial conditions
13 (Chen et al., 2011), which are usually difficult to accurately configure and may change rapidly
14 in developing countries.

15 Based on these urban canopy schemes, a series of modeling studies have investigated the
16 effects of urban land-use changes on regional climate and air quality. Some key climatic
17 effects of urbanization, e.g., an increase in mean surface temperature and PBL height, and
18 decrease in humidity and wind speed, have been captured (e.g. Wang et al., 2012; Wang et al.,
19 2013; Yang et al., 2012; Zhang et al., 2010), which in turn influence the concentrations of
20 pollutants even if the anthropogenic emissions are held constant (Civerolo et al., 2007; De
21 Meij et al., 2015; Wang et al., 2009; Yu et al., 2012). For instance, Kallos et al. (1993)
22 indicated that land surface conditions play an important role in the development of local
23 circulation and planetary boundary layer (PBL) depth, and could govern the dispersal,
24 transformation, and eventual removal of airborne pollutants. In addition, Ryu et al. (2013)
25 found that the prevailing urban breeze in the afternoon brought O₃-rich and biogenic VOC-
26 rich air masses from surrounding mountainous areas to the high-NO_x urban regions, resulting
27 in a very high ozone episode in the Seoul metropolitan area.

28 To date, the characteristics and intrinsic mechanisms of the forcing exerted by urban land
29 expansion on the atmospheric environment, including the burden of both primary and
30 secondary pollutants, are still not well understood, particularly throughout Eastern China.
31 Recently, the Chinese government has relaxed its one-child policy to promote the long-term
32 balanced development of the population, and has also launched an ambitious urbanization

1 campaign. Therefore, it is expected that China will undergo continuous urban population
2 growth and rapid urban land expansion in the coming decades. Land-use changes caused by
3 new urban infrastructure are usually irreversible. If urban land expansion exerts adverse
4 forcing on the ambient environment, mitigation strategies for climate and air quality
5 improvement would be less easily implemented and more costly.

6 Using WRF/Chem, a mesoscale fully coupled air quality and meteorological model, this study
7 addresses two key questions: 1) how sensitive are the meteorological conditions and the
8 spatial distribution of airborne contaminants to urban land expansion? 2) what are the intrinsic
9 mechanisms and dominant processes that drive urbanization induced changes in climate and
10 atmospheric chemistry? We describe the methodology and the model in section 2, and
11 evaluate the model results in Section 3. In section 4, we present the impact of urban land
12 expansion on the distribution of key atmospheric species. In section 5, we investigate the
13 individual processes contributing to these changes in atmospheric composition. Conclusions
14 are provided in section 6.

15 **2 Methodology**

16 **2.1 Model description and configuration**

17 We use WRF/Chem v3.5 (Grell et al., 2005) to simulate meteorological fields and
18 atmospheric chemistry under four hypothetical urban land surface expansion scenarios in July
19 for the five years from 2008 to 2012. We focus on summertime air quality because of the high
20 ozone and other secondary pollutants levels. The modeling framework is constructed on a
21 single domain of 100×100 cells with a 10 km horizontal grid spacing, and covers nine
22 provinces in eastern and central China (Figure 1). In this study, the physical options include
23 the Lin microphysics scheme (Lin et al., 1983), RRTM longwave radiation scheme (Mlawer
24 et al., 1997), Goddard shortwave scheme (Kim and Wang, 2011), MM5 M-O surface layer
25 scheme (Chen and Dudhia, 2001), YSU boundary layer scheme (Hong et al., 2006), New
26 Grell cumulus scheme, and Unified Noah land surface model (Chen and Dudhia, 2001). The
27 chemical options include the RADM2 chemical mechanism, MADE/SORGAM aerosol
28 scheme, Madronich F-TUV photolysis scheme, and Megan biogenic emission scheme
29 (Guenther et al., 2006). The $1.0^\circ \times 1.0^\circ$ NCEP Final Operational Global Analysis data
30 (<http://rda.ucar.edu/datasets/ds083.2/>) have been processed to provide the meteorological
31 initial conditions (IC) and boundary conditions (BC). We utilize the modified 2008 IGBP

1 (International Geosphere Biosphere Programme) MODIS 20-category 30 s land-use data,
 2 which is available from the WRF website (<http://www2.mmm.ucar.edu/wrf/users/>), to
 3 represent current land cover conditions. Anthropogenic emission data are from Multi-
 4 resolution Emission Inventory for China (MEIC) developed by Tsinghua University for the
 5 year 2010, which consists of the emission rates for each month from five sectors (agriculture,
 6 industry, power plants, residential and transportation). The MEIC is a unit/technology based,
 7 bottom-up emission model that covers ~700 anthropogenic emission source categories in
 8 China. It is an update of the emission inventory developed by the same group (Lei et al., 2011;
 9 Zhang et al., 2009). We used the MEIC 2010 data of the corresponding month as input for all
 10 simulations of 2008 through 2012, ignoring the year-to-year variation in emissions.

11 Predicted hourly ground level concentrations of CO, O₃, and particulate matter with
 12 aerodynamic diameter less than 2.5 microns (PM_{2.5}) are examined against observations made
 13 at five environmental monitoring sites, namely Nanjing Zhonghuamen Site (NJ_ZHM,
 14 118.78 °E, 32.01 °N), Nanjing Xianlin Site (NJ_XL, 118.91 °E, 32.11 °N), Hangzhou Jiande
 15 Site (HZ_JD, 119.28 °E, 29.46 °N), Hangzhou Yuhang Site (HZ_YH, 119.99 °E, 30.26 °N) and
 16 Shanghai Pudong Site (SH_PD, 121.55 °E, 31.22 °N), as shown in Figure 1. NJ_ZHM and
 17 NJ_XL are located in a mixed residential–educational area of Nanjing City, and the
 18 observation data (July 2012) are provided by Nanjing Municipal Environmental Monitoring
 19 Center. As NJ_ZHM and NJ_XL are located very close, and cannot be distinguished at the
 20 current model resolution, we average the observation data of these two sites and report it as
 21 NJ. Both HZ_JD and HZ_YH are located at high schools in Hangzhou City, and the relevant
 22 observation data (April 2008) are from Jiang et al. (2012). SH_PD is located in the urban
 23 center of Pudong District, Shanghai, and relevant observation data (September 2012) are from
 24 Tie et al. (2013). Extra simulations for April 2008 and September 2012 have been conducted
 25 for the purpose of model evaluation. The model performance is assessed by computing four
 26 conventional statistical metrics: the correlation coefficient (R), normalized mean bias (NMB),
 27 normalized mean error (NME), and index of agreement (I), which are defined as follows:

$$28 \quad R = \frac{\sum_{i=1}^N (p_i - \bar{p})(o_i - \bar{o})}{\sqrt{\sum_{i=1}^N (p_i - \bar{p})^2 \cdot \sum_{i=1}^N (o_i - \bar{o})^2}} \quad (1)$$

$$1 \quad NMB = \frac{\sum_{i=1}^N (p_i - o_i)}{\sum_{i=1}^N o_i} \times 100\% \quad (2)$$

$$2 \quad NME = \frac{\sum_{i=1}^N |p_i - o_i|}{\sum_{i=1}^N o_i} \quad (3)$$

$$3 \quad I = 1 - \frac{\sum_{i=1}^N (p_i - o_i)^2}{\sum_{i=1}^N (|p_i - \bar{o}| + |o_i - \bar{o}|)^2} \quad (4)$$

4 where p_i , o_i , and N represent model predicted data, observational data, and the number of data
 5 pairs, respectively. Eq. 4 indicates that I is a positive value no greater than 1, the larger the
 6 value of I , the better the model performs, and a value of 1 indicates a perfect match between
 7 the model and observations.

8 **2.2 Scenarios of urban land expansion**

9 This work investigates the sensitivity of climatic conditions and atmospheric chemical fields
 10 to changes in urban land cover on a regional scale. Four idealized urban land surface
 11 expansion scenarios are designed within the WRF/Chem modeling framework by modifying
 12 certain static geographical parameters. The land-use fraction by category describes the
 13 percentage coverage of different land-use categories within a given grid cell, and the land-
 14 use index indicates the grid's dominant land-use category. The BASE run uses the prescribed
 15 2008 IGBP MODIS 20-category land-use data. The GE0.2 run converts all cells with an
 16 urban land-use fraction of 0.2 or more to urban land-use index. The GE0.1 (urban land-use
 17 fraction ≥ 0.1) and GT0 (urban land-use fraction > 0) urban expansion scenarios are
 18 constructed similarly. Note that only the land-use index has been modified since the Noah
 19 land surface model considers only land-use index rather than a mosaic of multiple land-use
 20 categories with various land-use fractions. Figure 1 shows a schematic map of the four
 21 idealized urban land expansion scenarios (i.e., BASE, GE0.2, GE0.1, and GT0). The urban
 22 land surface expands extensively over the Yangtze River Delta, and most newly urbanized
 23 regions aggregate around the periphery of the original urban districts. Figure S1 (in the
 24 supplementary materials) shows the original dominant land-use categories of newly
 25 urbanized cells in the GT0 run, as well as a contour map of terrain height in the domain of

1 interest. Most new urban areas emerge to replace cropland, whereas few appear in
2 mountainous areas.

3 **2.3 Integrated process rate analysis**

4 In Eulerian grid air quality models such as WRF/Chem and CMAQ, the numerical technique
5 of operator splitting is used to solve the governing equations for species' concentrations.
6 Operator splitting involves separating the continuity equation for each species into several
7 simpler partial differential equations or ordinary differential equations consisting of one or
8 two individual processes (Gipson, 1999). The technique of integrated process rate (IPR)
9 analysis has been developed to track the accumulated contributions of individual physical
10 and chemical processes to model predictions during runtime. IPR has already been fully
11 implemented in CMAQ, and recent studies have reported its use in investigating a high
12 ozone episode in the Yangtze River Delta (Li et al., 2012) and the Pearl River Delta (Wang
13 et al., 2010), China, as well as the fate of major airborne pollutants in the southeastern US
14 (Yang and Shiang-Yuh, 2013).

15 However, IPR has not yet been officially adopted in the WRF/Chem modeling framework.
16 Jiang et al. (2012) added a simple process analysis scheme to WRF/Chem to calculate the
17 contribution of photochemical and physical processes to O₃ formation. In this paper, we
18 extend this work by implementing an improved online IPR scheme in WRF/Chem to track
19 contributions from 10 processes, namely horizontal and vertical advection (ADVH and
20 ADVZ), emissions (EMISS), dry deposition (DRYDEP), turbulent diffusion (DIFF),
21 convection (CONV), gas phase chemistry (CHEM), cloud chemistry (CLDCHEM), aerosol
22 processes (AERCHEM), and wet scavenging (WETSCAV). The calculation of dry
23 deposition is based on resistance models for gaseous species (Wesely, 1989) and particles
24 (Ackermann et al., 1998). Note Zhang and He (2014) recently developed a new algorithm
25 that linked dry deposition of particles with canopies via leaf area index (LAI), which is not
26 included in the version of WRF/Chem used in this study. Cloud chemistry refers to aqueous-
27 phase processes in different types of clouds, and aerosol processes refer to microphysical
28 nucleation, condensation, and coagulation. Convective scavenging refers to in-cloud rainout
29 within wet convective updrafts (subgrid processes), whereas wet scavenging refers to below-
30 cloud washout during large-scale precipitation. In the modal aerosol scheme
31 MADE/SORGAM (Ackermann et al., 1998; Schell et al., 2001), PM_{2.5} comprises Aitken and
32 accumulation mode particles of sulfate, nitrate, ammonium, organic carbon (including SOA)

1 and black carbon. The process contribution is calculated by subtracting the species burden of
2 each cell before and after each process is simulated. In WRF/Chem, dry deposition is
3 intermingled with vertical diffusion, so changes in the column burden during vertical mixing
4 can be attributed to dry deposition. The IPR technique is verified by comparing the changes
5 in species burden with the sum of contributions from the 10 processes mentioned above
6 during each model output interval. As shown in Figure S2, the net contribution of these 10
7 processes broadly matches the species concentration change.

8 **3 Model evaluation**

9 Figure 2 compares simulated versus observed daily mean surface concentrations of O₃, CO,
10 and PM_{2.5} over five monitoring sites: NJ_ZHN (07/2012), NJ_XL (07/2012), SH_PD
11 (09/2009), HZ_YH (04/2008), and HZ_JD (04/2008). The comparison indicates that
12 WRF/Chem is capable of capturing the daily mean concentrations of surface O₃ (R = 0.66;
13 NME = 27%), CO (R = 0.74; NME = 41%), and PM_{2.5} (R = 0.63; NME = 29%). Recent
14 evaluation of the ensemble of regional air quality models in the Air Quality Model
15 Evaluation International Initiative (AQMEII) indicated that, modeling of PM_{2.5} suffered from
16 too low variability and underestimation (Im et al., 2014; Solazzo et al., 2012). However, in
17 this study the daily mean observed and modeled PM_{2.5} concentrations in NJ sites are $47.4 \pm$
18 22.7 and 51.3 ± 29.0 $\mu\text{g}/\text{m}^3$, while in SH_PD site are 41.8 ± 12.3 and 44.1 ± 21.0 $\mu\text{g}/\text{m}^3$,
19 respectively. Both the mean and daily variability (indicated by the ratio of the standard
20 deviation of the measurements to the standard deviation of the model) of PM_{2.5}
21 concentrations are overestimated a bit. The modeled and observed hourly concentrations of
22 O₃, CO, and PM_{2.5} at above five sites are also compared for the whole month. WRF/Chem
23 generally captures the diurnal variation of surface O₃ well, (i.e., R: 0.74, NMB: 6.7%, NME:
24 34.1 %, and I: 0.86). The model also reproduces the hourly surface burden of PM_{2.5} and CO,
25 with NMEs of 63.4% and 52.6%, respectively. In addition, WRF/Chem captures the monthly
26 mean surface concentrations of O₃, CO, and PM_{2.5} fairly well (although O₃ in SH is over-
27 predicted by 17% and CO in NJ is under-predicted by 30%). A number of previous air
28 quality studies have evaluated the performance of WRF/Chem in simulating a range of
29 chemical species (e.g., PM_{2.5}, CO, and O₃) over China (Li et al., 2012; Tie et al., 2013; Tie et
30 al., 2007), and these have reported similar results.

1 4 Impacts of urban land expansion on regional atmospheric environment

2 4.1 Urbanization-induced concentration changes

3 Urban land expansion significantly alters the local synoptic conditions (see Figure S3 in the
4 supplementary materials), e.g., an increase in 2-meter temperature and boundary layer height,
5 and a decrease in 2-meter relative humidity and 10-meter wind speed (, could be different for
6 regions where urban land cover replaces forests). Changes in meteorology impact ambient air
7 quality, even when anthropogenic emissions remain constant. We focus on the response of
8 two gaseous species (i.e., CO and O₃) and two aerosol species (i.e., EC and PM_{2.5}). EC and
9 CO are used to study how urban land expansion would impact the dispersion and dilution of
10 primary pollutants. EC includes Aitken-mode EC (ECI) and accumulation-mode EC (ECJ),
11 and the aerosol scheme simulates the aging process by converting ECI to ECJ. O₃ and PM_{2.5}
12 are used to further investigate the effects of urban land expansion on secondary pollutants.

13 The model surface layer (Figure 3) and 800 hPa layer (Figure 4) are selected to study the 5-
14 year mean concentrations in July of CO, EC, O₃, and PM_{2.5} under the four urbanization
15 scenarios. In the BASE run, high levels of surface CO (~850–1250 ppb), EC (~9–13 μg m⁻³),
16 and PM_{2.5} (~90–130 μg m⁻³) are found only in urban areas where anthropogenic emissions
17 are high. In contrast, terrestrial O₃ (~24–32 ppb) is more evenly distributed on the regional
18 scale. At 800 hPa, concentrations of CO (~40–70 ppb), EC (~0.2–0.4 μg m⁻³), O₃ (~24–30
19 ppb), and PM_{2.5} (~10–20 μg m⁻³) over the North China Plain appear much higher than those
20 in the southern domain, consistent with the satellite-observed pollution distribution features
21 over this domain (e.g. Liu et al., 2013). A one-tailed student *t*-test (based on the standard
22 error computed from hourly variability) is used to determine whether the assumed expansion
23 of urban land causes changes in local monthly mean concentrations that are significant at the
24 95% confidence level. In the surface layer, the change in dominant land-use type to urban
25 generally induces a significant decrease in surface concentrations of CO (up to -44%;
26 domain-wide average of -11%, or up to 40 ppb decrease in the GT0 run), EC (up to -80%;
27 domain-wide average of -21%, or -0.3 μg m⁻³ in the GT0 run), and PM_{2.5} (up to -74%;
28 domain-wide average of -21%, or -5.4 μg m⁻³ in the GT0 run) in all urbanization scenarios.
29 However, the changes in surface O₃ are generally insignificant in GE0.2. Urban land
30 expansion leads to a moderate increase in surface O₃ (maximum of 22%; domain-wide
31 average of 0.3%, equivalent to 0.1 ppb in the GT0 run) over the northern terrestrial domain
32 in the GE0.1 and GT0 runs. At 800 hPa, the expansion of urban land significantly increases

1 the local concentrations of CO (with a domain-wide average of 16%, and up to 5.6 ppb in the
 2 GT0 run), EC (domain-wide average of 50%, or $\sim 0.05 \mu\text{g m}^{-3}$ in the GT0 run), O₃ (domain-
 3 wide average of 16%, or ~ 2.8 ppb in the GT0 run), and PM_{2.5} (domain-wide average of 65%,
 4 or $\sim 4.3 \mu\text{g m}^{-3}$ in the GT0 run) in the different urbanization scenarios. The effect of urban
 5 land expansion on CO, EC, O₃ and PM_{2.5} concentrations is consistent in each year, albeit
 6 with slight differences in magnitude (not shown).

7 **4.2 Linearity of urbanization-response relationship over East China**

8 The urbanization-response relationship is a complex function of local synoptic conditions,
 9 large-scale circulation, land surface type, the physical and chemical properties of an airborne
 10 contaminant and its emissions (e.g., release height, frequency, and amount), as well as the
 11 time scale being considered. The strength of urban land forcing (e.g., the sensitivity of an
 12 atmospheric variable to urban land expansion) can be quantitatively evaluated as the
 13 perturbation of this variable from its base condition. Figure 5 shows the response of the 5-year
 14 mean concentrations in July of CO, EC, O₃, and PM_{2.5} to changes in domain-wide (i.e., East
 15 China) urban land coverage. At both the surface and 800 hPa, the response curves are
 16 nonlinear and the rate of domain-wide concentration changes decreases as more urban land
 17 emerges. However, as shown in Figures 3 and 4, the concentration response is nonuniformly
 18 distributed, and becomes stronger when large tracts of new urban land appear. This indicates
 19 that the aggregation state (further discussed in the next paragraph) of newly urbanized areas
 20 would alter the strength of urban land forcing.

21 The forcing effect of urban land expansion on the spatial distribution of air pollutants is not
 22 usually limited to newly urbanized areas, but has a distance of extended influence. To
 23 differentiate the shape of urbanization-response curves at different locations, we use LOCAL
 24 to denote these newly urbanized cells, and ADJACENT to represent the non-urbanized cells
 25 neighboring LOCAL. We further define an aggregation parameter (Agg) for a given LOCAL
 26 cell as the number of the surrounding cells that are also LOCAL; we limit the number of
 27 surrounding grid cells for this analysis to $5 \times 5 - 1$ or 24 cells (2400 km²). The “local” or
 28 “adjacent” forcing is defined as:

$$29 \quad f_j = \frac{\sum_{i=1}^{N_j} \frac{VC_i}{VB_i}}{N_j} \quad (5)$$

1 where f_l (i.e., $j = 1$) denotes local forcing (LF), N_l is the number of domain-wide LOCAL
2 cells, VC_i and VB_i denote the values of a certain atmospheric variable in cell i of the
3 perturbation run and the BASE run, respectively. f_2 denotes adjacent forcing (AF) over the
4 ADJACENT cells, and N_2 is the number of domain-wide ADJACENT cells.

5 Figure 6 illustrates the LF and AF induced by urban land expansion (i.e., the perturbation of
6 5-year mean in July concentrations of CO, EC, O₃, and PM_{2.5} from the BASE situation) in all
7 three idealized urbanization scenarios. At the surface, the relationship between LF and Agg is
8 nearly linear. Each 10% increase in Agg is associated with 1.6%, 1.8%, and 2.2% decreases in
9 LOCAL CO, EC, and PM_{2.5} concentrations, respectively, and a 1% increase in O₃
10 concentrations. The AF-Agg curves are similar to those for LF-Agg, but have weaker
11 responses. The linearity can be explained as follows: with increasing Agg, there are more
12 LOCAL cells near a given cell, so the same number of adjacent effects are added to the given
13 cell. At 800 hPa, changes in the contaminant burden seem to be more sensitive to the
14 aggregation level of newly urbanized cells than at the surface, and particles seem to be more
15 susceptible than gases. The associated urbanization-response curves become nonlinear. It can
16 be observed that both LF and AF are linearly associated with the square of Agg, which means
17 each 10% increase in the square of Agg may enhance air pollution concentrations by about 5–
18 10% at 800 hPa, with the maximum sensitivity for PM_{2.5} (12%). This indicates that dense
19 urbanization over East China may have a moderate dilution effect on surface air pollution, but
20 could intensify pollutants aloft and therefore severe haze (i.e. visibility degradation) and
21 ozone pollution if local emissions are not reduced in the future.

22 Besides the response of air pollutants, we found that the perturbations in July-mean boundary
23 layer height, 2-meter temperature, and 2-meter relative humidity also increase linearly with
24 Agg ($R^2 > 0.96$, shown in Figure S4 in the supplementary materials). These results indicate
25 that when large tracts of new urban land emerge, impacts of land cover change on
26 meteorology and air pollutant concentrations can be magnified.

27 **5 Mechanism governing the urbanization-response relationship**

28 **5.1 Process contribution to surface air quality changes**

29 Figure 7 shows the 5-year mean in July diurnal cycles of CO, EC, O₃, and PM_{2.5} surface
30 concentrations averaged over the domain-wide LOCAL cells and the ADJACENT cells. At
31 the surface, CO, EC, and PM_{2.5} share a diurnal variation pattern in which concentrations peak

1 at dawn (~05:00 LST) and reach a trough in the late afternoon (~16:00 LST). Concentrations
2 over LOCAL cells are usually higher than those over the ADJACENT regions, particularly
3 during the night. However, for O₃, the opposite diurnal variation pattern can be observed, and
4 the difference between LOCAL and ADJACENT cells is small. Urban land expansion leads
5 to substantial changes in species concentrations, but has little effect on the shape of the
6 diurnal cycle. As urban land expands, CO, EC, and PM_{2.5} tend to evolve toward lower burden
7 levels. In contrast, when averaged over the domain, the increment in surface O₃
8 concentrations during most of the day is insignificant. Though the resulting concentration
9 changes in LOCAL and ADJACENT are quite similar for these four species, the IPR analysis
10 suggests that the underlying mechanisms that drive the forcing–response relationship are
11 different.

12 Figure 8 illustrates the 5-year mean in July diurnal cycles of IPR contributions in the BASE
13 run and their deviations in the GT0 run over the domain-wide surface LOCAL cells and
14 ADJACENT cells. The daytime period is chosen as 07:00–18:00 LST, with the rest of the day
15 considered to be nighttime. In the BASE run, emissions are the dominant source of CO over
16 the LOCAL cells, and the dominant sink is turbulent transport (daytime advection is also a
17 contributing sink). EC follows a similar IPR pattern to CO, except that dry deposition is also a
18 major sink, accounting for about 40% of the total EC removal. Since this study considers
19 constant CO and EC emissions, diurnal variability in concentrations is dominated by
20 variations in the strength of vertical transport. During the daytime, vertical transport is strong,
21 and CO and EC are depleted at the surface. However, during the nighttime, vertical transport
22 becomes weaker, which allows CO and EC to accumulate. The diurnal cycle of IPR for PM_{2.5}
23 is very similar to that of EC, but aerosol processes play an important role. During the daytime,
24 the source of PM_{2.5} is dominated by surface emissions, but the sinks are quite complicated,
25 including turbulent diffusion (~41%), dry deposition (~36%), and aerosol processes (~23%).
26 Note that by conducting IPR analyses within CMAQ, Yang and Shiang-Yuh (2013) found
27 that aerosol processes depletion can act as a sink for PM_{2.5}. At night, the production of PM_{2.5}
28 through aerosol processes forms 22% of the source. The IPR diurnal cycle for O₃ is quite
29 different. During the daytime, the major sources for surface O₃ are photochemical production
30 (~37%) and turbulent transport (~63%), and the sink is overwhelmingly dry deposition. At
31 night, removal of O₃ through gas-phase reactions and dry deposition accounts for 40% and
32 60% of the sink, respectively. The diurnal cycles of IPR contribution over the ADJACENT
33 cells are similar to those of LOCAL cells, except that vertical diffusion becomes a source for

1 PM_{2.5} during the daytime, compensating for the strong loss by aerosol processes and dry
2 deposition.

3 In the GT0 run, as urban land expands, changes in horizontal (vertical) advection tend to
4 increase (reduce) the surface concentration of all four species over the LOCAL cells, whereas
5 the opposite is true for the ADJACENT cells. The associated surface wind field perturbations
6 due to urban land expansion are shown in Figure 9. The urban land expansion could
7 strengthen the southeasterly sea breeze over marine and near the east seaboard of China, due
8 to the increased difference in thermal properties between land and sea (as the urban land is
9 characterized with a greater heat capacity, thermal conductivity and lower albedo). However,
10 perturbation of wind field in the inner terrestrial is more complicated, generally speaking, the
11 replacement of natural land by urban land would reduce the local pressure (up to 30 Pa) and
12 form a cyclonic convergence zone. The divergence of the perturbed wind field can be
13 calculated by a centered finite difference scheme with a one-sided difference boundary.
14 Values of convergence up to $-6 \times 10^{-5} \text{ s}^{-1}$ can be observed in most of the newly urbanized areas,
15 similar to the results of Bornstein and Lin (2000), who concluded that UHI would induce a
16 convergence ($\sim -10^{-5} \text{ s}^{-1}$) zone over Atlanta. Figure 10 shows the perturbed wind field in the
17 three vertical–longitudinal cross-sections of CS1, CS2, and CS3 mentioned in Figure 1. The
18 emergence of urban land induces local updrafts of $\sim 1 \text{ cm s}^{-1}$, which enhances the ventilation
19 of primary pollutants to the free troposphere; adjacent downdrafts are also observed. The
20 perturbed wind induced by urban land expansion generally forms convergence zones above
21 the LOCAL cells and divergence zones over the ADJACENT cells (Figure 9). Urban heat
22 island circulation (UHIC) is enhanced, which explains the changes in the contribution of
23 advection.

24 The effects of urban land expansion are not limited to the UHIC-induced advection changes.
25 In the surface layer, the vertical diffusion of CO is intensified over LOCAL cells (especially
26 during the night). EC differs from CO in that the loss due to dry deposition markedly
27 increases over the entire day, while the sink due to diffusion is only reduced during the
28 daytime but is increased at night. The sum of dry deposition and turbulent diffusion reflects
29 the role of vertical mixing in relocating the airborne pollutants vertically. The sink due to the
30 vertical mixing of EC is intensified. It can be concluded that the enhanced advection and
31 turbulent mixing in the vertical direction are the key factors in reducing the surface
32 concentrations of CO and EC. For O₃, dry deposition, vertical diffusion, and daytime

1 photochemical production and nighttime chemical depletion are all reduced at the surface,
2 resulting in a net weak enhancement of surface O_3 averaged over domain-wide LOCAL cells.
3 The dry deposition of O_3 is reduced because the canopy resistance increases as vegetation is
4 replaced by urban land; however, the dry deposition of particles is not impacted by canopy
5 resistance, but is rather fostered by the intensified surface turbulence. Vertical diffusion is
6 possibly hindered by convergent updrafts caused by UHIC, and the daytime photochemical
7 production and nighttime chemical depletion are reduced because of the decreased abundance
8 of precursors. For $PM_{2.5}$, daytime loss and nighttime production via aerosol processes are
9 enhanced and hindered, respectively, this may be because the urbanization-induced decrease
10 in precursor concentrations restrains gas-to-particle mass transfer. At the same time, dry
11 deposition and vertical diffusion are also enhanced during the daytime. Therefore, the
12 increased sink resulting from aerosol processes and dry deposition is the key factor reducing
13 $PM_{2.5}$ concentrations at the surface. Over the ADJACENT cells, urbanization-induced
14 outward horizontal advection contributes to the lower burden of CO, EC, and $PM_{2.5}$, and the
15 sink term due to vertical mixing decreases.

16 **5.2 Urbanization-induced process-level vertical profile changes**

17 Figure 11 shows the 5-year mean in July vertical profile of the four species averaged in the
18 domain-wide LOCAL and ADJACENT cells of the BASE and GT0 runs. In both types of
19 cells, CO, EC, and $PM_{2.5}$ exhibit similar patterns; as urban land expands, the atmospheric
20 burden decreases near the surface (below 1 km), but increases at higher altitudes (1–4 km).
21 On the other hand, the concentration of O_3 increases at most heights from the surface to a
22 height of about 4 km. Unlike near the surface, the magnitude of the concentration
23 perturbations aloft (1–4 km) in both grids is commensurate with the atmospheric burden.

24 Figure 12 illustrates the vertical profile of 5-year mean in July daytime and nighttime IPR
25 contributions for CO, EC, O_3 , and $PM_{2.5}$ in the BASE and GT0 runs, averaged over all
26 LOCAL cells. Convective scavenging generally plays a minor role in removing these four
27 species. For CO and EC, vertical mixing and advection play key roles in constraining the
28 vertical profiles, and the net diffusion is unidirectional from the ground to higher altitudes.
29 The extent of vertical transport during the daytime is higher than that during nighttime. The
30 forcing of urban land expansion on the transport of primary pollutants is characterized by
31 UHIC-induced advection changes and enhanced vertical mixing, leading to the decreased
32 vertical concentration gradient (as shown in Figure 11). A positive perturbation in the

1 horizontal advection contribution and a negative perturbation in the vertical advection
2 contribution are found in the lower atmosphere (below 500 m), whereas the opposite is true in
3 the upper atmosphere (~0.5–3 km), similar to the Ekman pump. For CO and EC (only during
4 nighttime), the enhanced sink and source due to vertical mixing in lower and upper
5 atmosphere, respectively, could be the key reasons for changes of vertical profile, and
6 advection appears to compensate and balance this effect. However, for EC above 1 km, as
7 surface dry deposition is strengthened markedly in the daytime, whereas diffusion from the
8 lower atmosphere is dampened; this is compensated by the enhanced upward advection.

9 For O₃, advection, vertical mixing, and gas-phase reactions all play important roles in
10 constraining its vertical profile. Though UHIC-induced horizontal and vertical advection
11 changes cause the IPR to shift significantly across all layers, net advection is not the key
12 process driving the changes in the vertical O₃ profile. Near the ground level, the expansion of
13 urban land fosters upward diffusion and hinders downward diffusion to the surface layer. O₃
14 production is determined by the availability of precursors, which is increased in the 1–3 km
15 zone by the enhanced uplifting of primary pollutants. The dampened dry deposition and
16 enhanced daytime photochemical production (at around 0.5–3 km) are responsible for a
17 higher O₃ profile.

18 Besides the transport of precursors, other meteorological factors may also influence O₃
19 production. The bottom three plots in Figure 10 show the distribution of chemical production
20 (ppb/h), cloud water, and air temperature differences (GT0 minus BASE during the period
21 12:00–17:00 LST) in the cross-sections of CS1, CS2, and CS3 (defined in Figure 1). As urban
22 land expands, air temperatures increase (up to 1.2 °C) in the lower layers (below 0.5 km), but
23 decrease slightly above 2 km. However, photochemical production of O₃ is intensified only at
24 altitudes higher than 2 km. This indicates that changes in air temperature may not be the
25 principal factor determining O₃ production above the PBL. As shown in Figure 10, the
26 locations of newly urbanized cells exactly match the zones where photochemical production
27 of O₃ is reduced in lower layers but cloud water content is significantly increased above 1 km.
28 Low altitude clouds efficiently scatter shortwave radiation, thus hindering photochemical
29 reactions below clouds; thus, urban land forcing indirectly effects the spatial distribution of
30 O₃.

31 As shown in Figure 12, aerosol chemistry, vertical mixing, and advection all contribute
32 strongly to constraining the PM_{2.5} vertical profile, with wet scavenging and cloud chemistry

1 playing relatively minor roles. During the daytime, the contribution of aerosol chemistry is
2 negative near the surface, but turns positive at higher altitudes. At night, the contribution of
3 aerosol chemistry remains positive in all vertical layers. The net vertical turbulent transport is
4 upward in the surface layer, but reverses to downward above 0.5 km. Similar to O₃, as urban
5 land expands, changes in the vertical profiles of precursors result in enhanced aerosol
6 production at 0.5–3 km, and enhanced loss below 0.5 km (where the downward diffusion is
7 intensified). The perturbation of dry deposition and aerosol processes largely explains the
8 PM_{2.5} vertical profile changes. Alike the case for the photochemical formation of O₃, the
9 formation of PM_{2.5} through gas phase/particle partitioning and cloud chemistry is also
10 influenced by the relocation of humidity, as simulated by the MADE/SORGAM scheme
11 (Please refer to the supplementary materials for details). As shown in Figure S5 in the
12 supplementary materials, the production of PM_{2.5} through cloud chemistry increase (decreases)
13 exactly where the humidity increases (decreases).

14 The caveats of this study are as follows: 1) The forcing of urban land expansion on the
15 atmospheric environment is confined to the regional scale. Feedback between mesoscale
16 circulation and large-scale circulation, as well as inflows of airborne pollutants from outside
17 the domain of interest, has been ignored. 2) It is important to note that emissions are assumed
18 to remain constant during our study time period. We chose constant emissions to ensure we
19 could tease out the effects of land-cover induced changes on air quality without confounding
20 changes in emissions. Sensitivity experiments show that, at surface, the diluting effects of
21 urban land could be offsetted only if the emission augment is high enough for CO (~40%) and
22 EC (~100%) in LOCAL cells (see Figures S6-S8 in the supplemental materials for details). 3)
23 The BULK urban canopy scheme used in this work does not resolve the urban morphology,
24 and therefore cannot further investigate how urban canopy parameters, such as the building
25 height and anthropogenic heat, would impact the climatic conditions and air quality. The
26 urbanization-response relationship unveiled in this work could be urban scheme dependent. In
27 future studies, we will focus on addressing these effects to better quantify the urbanization–
28 response relationship, which could provide support to urban planning.

29 **6 Conclusions**

30 We have used an online coupled mesoscale meteorology-chemistry model (WRF/Chem) with
31 BULK urban scheme embodied in Noah land surface model and an improved integrated
32 process rate (IPR) analysis scheme to study the effects of urban land expansion in eastern

1 China on climate and air quality during the month of July. Urban land expansion could
2 significantly alter local synoptic conditions (e.g., increases in 2-meter air temperature and
3 boundary layer height and decreases in 2-meter relative humidity). Above the newly
4 urbanized grid cells (referred to as LOCAL cells), horizontal perturbations in wind form
5 cyclonic convergence ($\sim 10^{-5} \text{ s}^{-1}$) zones, and vertical perturbations in wind lead to updraft
6 flows ($\sim 1 \text{ cm/s}$). This urbanization-induced circulation consequently impacts ambient air
7 quality, even when surface emissions remain constant. For primary pollutants with strong
8 surface emissions (e.g., CO and EC), urban land expansion causes concentrations to decrease
9 below 500 m but increase significantly between 1 and 3 km. On the other hand, the O₃ burden
10 averaged over LOCAL cells consistently increases from the surface to about 4 km. For PM_{2.5},
11 though its source includes both primary emissions and secondary formation, the changes in
12 vertical profile caused by urban land expansion are consistent with those of CO and EC.

13 The effects of urban land expansion are not localized, but rather its influence extends to
14 neighboring areas. In this study, the local forcing (LF) was found to be significantly larger
15 than adjacent forcing (AF) at the surface, especially for particulate matter. The aggregation
16 state of newly urbanized areas plays an important role in determining the strength of LF and
17 AF. We found that perturbations of CO, EC, O₃, and PM_{2.5} change linearly with aggregation
18 parameter (Agg) at the surface, and with the square of Agg at 800 hPa ($R^2 > 0.94$). In addition,
19 the perturbations of mean July levels of boundary layer height, 2-meter temperature, and 2-
20 meter relative humidity increase linearly with Agg ($R^2 > 0.96$). This result indicates that when
21 large tracts of new urban land emerge, the effects of urban expansion on atmospheric physics
22 and chemistry are magnified.

23 IPR was utilized to investigate the forcing mechanisms exerted by urban land expansion on
24 the spatial distribution of CO, EC, O₃, and PM_{2.5} over the LOCAL cells. At the surface, a
25 common feature of all four species governed by the UHIC effect whereby horizontal
26 advection causes increases in concentrations and vertical advection causes decreases in
27 concentrations. Additionally, when natural vegetation was replaced by urban land, the sink
28 term from dry deposition increased for particles but decreased for gaseous species. For
29 primary pollutants CO and EC, enhanced advection and turbulent mixing in the vertical
30 direction are the key factors in reducing the surface concentrations. On the other hand, for
31 PM_{2.5}, increased sinks due to aerosol processes and dry deposition are the key factors in
32 reducing surface concentrations. For O₃, the reduced dry deposition and vertical diffusion, as

1 well as the relocation of precursors, played an important role in constraining the surface
2 concentration, resulting in a net enhancement of the surface O₃ averaged over all LOCAL
3 cells.

4 In contrast to the surface conditions, urban land expansion may induce substantial increases in
5 air pollution at higher altitudes. The positive contribution of vertical advection and the
6 negative contribution of horizontal advection were found to be important in the build-up of air
7 pollution in the upper atmosphere (0.5–3 km). For primary pollutants CO and EC (only during
8 nighttime), the enhanced uplifting caused by strengthened turbulent diffusion (induced by
9 urban land expansion) is the key factor leading to higher burdens in the upper atmosphere.
10 However, in daytime, diffusion of EC from the lower atmosphere is dampened due to
11 intensified dry deposition, which partially counters the concentration increases from enhanced
12 upward advection. However, for secondary species, O₃ and PM_{2.5}, the relocation of precursors
13 accelerates daytime chemical production in the upper atmosphere, which is the key factor in
14 the higher burden of secondary pollutants at a height of about 1–4 km.

15 Above analysis revealed the nonnegligible and unique role of urban land forcing in impacting
16 the advection, turbulent mixing and dry/wet removal of pollutants, and indicated that dense
17 urbanization has a moderate dilution effect on surface primary airborne contaminants, but
18 may intensify severe haze and ozone pollution if local emissions are not well controlled.
19 Further studies should consider changes in both the land use (using of a more complicated and
20 advanced urban canopy scheme) and emission simultaneously to better evaluate the potential
21 environmental influence of any urbanization campaign.

22

23 **Acknowledgements**

24 We thank three anonymous reviewers for their thoughtful comments and helpful suggestions.
25 This work was supported by funding from the National Natural Science Foundation of China
26 under awards 41222011, 41390240, and 41130754, the Research Project of the Chinese
27 Ministry of Education No. 113001A, the “863” Hi-Tech R&D Program of China under Grant
28 No. 2012AA063303, and the 111 Project (B14001).

29

1 **References**

- 2 Ackermann, I. J., Hass, H., Memmesheimer, M., Ebel, A., Binkowski, F. S., and Shankar, U.:
3 Modal aerosol dynamics model for Europe: Development and first applications, *Atmospheric*
4 *Environment*, 32, 2981-2999, 1998.
- 5 Arnfield, A. J.: Two decades of urban climate research: a review of turbulence, exchanges of
6 energy and water, and the urban heat island, *International journal of climatology*, 23, 1-26,
7 2003.
- 8 Britter, R., and Hanna, S.: Flow and dispersion in urban areas, *Annual Review of Fluid*
9 *Mechanics*, 35, 469-496, 2003.
- 10 Changnon, S. A.: Inadvertent weather modification in urban areas: Lessons for global climate
11 change, *Bulletin of the American Meteorological Society*, 73, 619-627, 1992.
- 12 Chen, F., and Dudhia, J.: Coupling an advanced land surface-hydrology model with the Penn
13 State-NCAR MM5 modeling system. Part I: Model implementation and sensitivity, *Monthly*
14 *Weather Review*, 129, 569-585, 2001.
- 15 Chen, F., Kusaka, H., Bornstein, R., Ching, J., Grimmond, C. S. B., Grossman-Clarke, S.,
16 Loridan, T., Manning, K. W., Martilli, A., Miao, S. G., Sailor, D., Salamanca, F. P., Taha, H.,
17 Tewari, M., Wang, X. M., Wyszogrodzki, A. A., and Zhang, C. L.: The integrated
18 WRF/urban modelling system: development, evaluation, and applications to urban
19 environmental problems, *International Journal of Climatology*, 31, 273-288, 10.1002/joc.2158,
20 2011.
- 21 Civerolo, K., Hogrefe, C., Lynn, B., Rosenthal, J., Ku, J. Y., Solecki, W., Cox, J., Small, C.,
22 Rosenzweig, C., Goldberg, R., Knowlton, K., and Kinney, P.: Estimating the effects of
23 increased urbanization on surface meteorology and ozone concentrations in the New York
24 City metropolitan region, *Atmospheric Environment*, 41, 1803-1818,
25 10.1016/j.atmosenv.2006.10.076, 2007.
- 26 Coceal, O., and Belcher, S.: A canopy model of mean winds through urban areas, *Quarterly*
27 *Journal of the Royal Meteorological Society*, 130, 1349-1372, 2004.
- 28 Cui, Y. Y., and de Foy, B.: Seasonal Variations of the Urban Heat Island at the Surface and
29 the Near-Surface and Reductions due to Urban Vegetation in Mexico City, *Journal of Applied*
30 *Meteorology and Climatology*, 51, 855-868, 10.1175/jamc-d-11-0104.1, 2012.
- 31 De Meij, A., Bossioli, E., Penard, C., Vinuesa, J., and Price, I.: The effect of SRTM and
32 Corine Land Cover data on calculated gas and PM10 concentrations in WRF-Chem,
33 *Atmospheric Environment*, 101, 177-193, 2015.
- 34 Di Sabatino, S., Solazzo, E., Paradisi, P., and Britter, R.: A simple model for spatially-
35 averaged wind profiles within and above an urban canopy, *Boundary-layer meteorology*, 127,
36 131-151, 2008.
- 37 Fan, H., and Sailor, D. J.: Modeling the impacts of anthropogenic heating on the urban
38 climate of Philadelphia: a comparison of implementations in two PBL schemes, *Atmospheric*
39 *Environment*, 39, 73-84, 2005.
- 40 Fernando, H., Lee, S., Anderson, J., Princevac, M., Pardyjak, E., and Grossman-Clarke, S.:
41 Urban fluid mechanics: air circulation and contaminant dispersion in cities, *Environmental*
42 *Fluid Mechanics*, 1, 107-164, 2001.

- 1 Fisher, B., Kukkonen, J., Piringer, M., Rotach, M. W., and Schatzmann, M.: Meteorology
2 applied to urban air pollution problems: concepts from COST 715, *Atmos. Chem. Phys.*, 6,
3 555-564, 10.5194/acp-6-555-2006, 2006.
- 4 Gipson, G. L.: Science algorithms of the EPA Models-3 community multiscale air quality
5 (CMAQ) modeling system: process analysis, 37 pp., 1999.
- 6 Grell, G. A., Peckham, S. E., Schmitz, R., McKeen, S. A., Frost, G., Skamarock, W. C., and
7 Eder, B.: Fully coupled "online" chemistry within the WRF model, *Atmospheric Environment*,
8 39, 6957-6975, 10.1016/j.atmosenv.2005.04.027, 2005.
- 9 Guenther, A., Karl, T., Harley, P., Wiedinmyer, C., Palmer, P., and Geron, C.: Estimates of
10 global terrestrial isoprene emissions using MEGAN (Model of Emissions of Gases and
11 Aerosols from Nature), *Atmospheric Chemistry and Physics*, 6, 3181-3210, 2006.
- 12 Harman, I. N., Barlow, J. F., and Belcher, S. E.: Scalar fluxes from urban street canyons part
13 II: model, *Boundary-Layer Meteorology*, 113, 387-410, 2004.
- 14 Heilig, G. K.: *World Urbanization Prospects: The 2011 Revision*, United Nations, Washington,
15 DC, 2012.
- 16 Hong, S.-Y., Noh, Y., and Dudhia, J.: A new vertical diffusion package with an explicit
17 treatment of entrainment processes, *Monthly Weather Review*, 134, 2318-2341, 2006.
- 18 Im, U., Bianconi, R., Solazzo, E., Kioutsioukis, I., Badia, A., Balzarini, A., Baró R., Bellasio,
19 R., Brunner, D., Chemel, C., Curci, G., Denier van der Gon, H., Flemming, J., Forkel, R.,
20 Giordano, L., Jiménez-Guerrero, P., Hirtl, M., Hodzic, A., Honzak, L., Jorba, O., Knote, C.,
21 Makar, P. A., Manders-Groot, A., Neal, L., Pérez, J. L., Pirovano, G., Pouliot, G., San Jose,
22 R., Savage, N., Schroder, W., Sokhi, R. S., Syrakov, D., Torian, A., Tuccella, P., Wang, K.,
23 Werhahn, J., Wolke, R., Zabkar, R., Zhang, Y., Zhang, J., Hogrefe, C., and Galmarini, S.:
24 Evaluation of operational online-coupled regional air quality models over Europe and North
25 America in the context of AQMEII phase 2. Part II: Particulate matter, *Atmospheric
26 Environment*, <http://dx.doi.org/10.1016/j.atmosenv.2014.08.072>, 2014.
- 27 Jiang, F., Zhou, P., Liu, Q., Wang, T., Zhuang, B., and Wang, X.: Modeling tropospheric
28 ozone formation over East China in springtime, *Journal of Atmospheric Chemistry*, 69, 303-
29 319, 10.1007/s10874-012-9244-3, 2012.
- 30 Kallos, G., Kassomenos, P., and Pielke, R. A.: Synoptic and mesoscale weather conditions
31 during air pollution episodes in Athens, Greece, *Boundary-Layer Meteorology*, 62, 163-184,
32 1993.
- 33 Kanda, M.: Progress in urban meteorology: A review, *J. Meteorol. Soc. Jpn.*, 85B, 363-383,
34 2007.
- 35 Kim, H.-J., and Wang, B.: Sensitivity of the WRF model simulation of the East Asian
36 summer monsoon in 1993 to shortwave radiation schemes and ozone absorption, *Asia-Pacific
37 Journal of Atmospheric Sciences*, 47, 167-180, 2011.
- 38 Kusaka, H., and Kimura, F.: Coupling a single-layer urban canopy model with a simple
39 atmospheric model: Impact on urban heat island simulation for an idealized case, *J. Meteorol.
40 Soc. Jpn.*, 82, 67-80, 10.2151/jmsj.82.67, 2004.
- 41 Lei, Y., Zhang, Q., He, K., and Streets, D.: Primary anthropogenic aerosol emission trends for
42 China, 1990–2005, *Atmospheric Chemistry and Physics*, 11, 931-954, 2011.

- 1 Li, L., Chen, C. H., Huang, C., Huang, H. Y., Zhang, G. F., Wang, Y. J., Wang, H. L., Lou, S.
2 R., Qiao, L. P., Zhou, M., Chen, M. H., Chen, Y. R., Streets, D. G., Fu, J. S., and Jang, C. J.:
3 Process analysis of regional ozone formation over the Yangtze River Delta, China using the
4 Community Multi-scale Air Quality modeling system, *Atmospheric Chemistry and Physics*,
5 12, 10971-10987, 10.5194/acp-12-10971-2012, 2012.
- 6 Liao, J., Wang, T., Wang, X., Xie, M., Jiang, Z., Huang, X., and Zhu, J.: Impacts of different
7 urban canopy schemes in WRF/Chem on regional climate and air quality in Yangtze River
8 Delta, China, *Atmospheric Research*, 145, 226-243, 2014.
- 9 Lin, C. Y., Chen, W. C., Chang, P. L., and Sheng, Y. F.: Impact of the Urban Heat Island
10 Effect on Precipitation over a Complex Geographic Environment in Northern Taiwan, *Journal*
11 *of Applied Meteorology and Climatology*, 50, 339-353, 10.1175/2010jamc2504.1, 2011.
- 12 Lin, Y.-L., Farley, R. D., and Orville, H. D.: Bulk parameterization of the snow field in a
13 cloud model, *Journal of Climate and Applied Meteorology*, 22, 1065-1092, 1983.
- 14 Liu, Y., Chen, F., Warner, T., and Basara, J.: Verification of a Mesoscale Data-Assimilation
15 and Forecasting System for the Oklahoma City Area during the Joint Urban 2003 Field
16 Project, *Journal of Applied Meteorology and Climatology*, 45, 912-929, 10.1175/jam2383.1,
17 2006.
- 18 Liu, Y., Junfeng, L., and Shu, T.: Interannual Variability of Summertime Aerosol Optical
19 Depth over east asia During 2000-2011: a Potential Influence from el nino Southern
20 Oscillation, *Environmental Research Letters*, 8, 044034 (044039 pp.)-044034 (044039 pp.),
21 10.1088/1748-9326/8/4/044034, 2013.
- 22 Luhar, A. K., Thatcher, M., and Hurley, P. J.: Evaluating a building-averaged urban surface
23 scheme in an operational mesoscale model for flow and dispersion, *Atmospheric Environment*,
24 88, 47-58, 2014.
- 25 Mage, D., Ozolins, G., Peterson, P., Webster, A., Orthofer, R., Vandeweerd, V., and Gwynne,
26 M.: Urban air pollution in megacities of the world, *Atmospheric Environment*, 30, 681-686,
27 1996.
- 28 Martilli, A., Clappier, A., and Rotach, M. W.: An urban surface exchange parameterisation
29 for mesoscale models, *Boundary-Layer Meteorology*, 104, 261-304,
30 10.1023/a:1016099921195, 2002.
- 31 Miao, S. G., Chen, F., Lemone, M. A., Tewari, M., Li, Q. C., and Wang, Y. C.: An
32 Observational and Modeling Study of Characteristics of Urban Heat Island and Boundary
33 Layer Structures in Beijing, *Journal of Applied Meteorology and Climatology*, 48, 484-501,
34 10.1175/2008jamc1909.1, 2009.
- 35 Mlawer, E. J., Taubman, S. J., Brown, P. D., Iacono, M. J., and Clough, S. A.: Radiative
36 transfer for inhomogeneous atmospheres: RRTM, a validated correlated - k model for the
37 longwave, *Journal of Geophysical Research: Atmospheres* (1984 - 2012), 102, 16663-16682,
38 1997.
- 39 Oke, T. R.: *Boundary Layer Climates* (2nd edition), Routledge, London, UK 1987.
- 40 Oke, T. R.: Towards better scientific communication in urban climate, *Theoretical and*
41 *Applied Climatology*, 84, 179-190, 2006.
- 42 Rosenfeld, D.: Suppression of rain and snow by urban and industrial air pollution, *Science*,
43 287, 1793-1796, 2000.

- 1 Rotach, M. W., Fisher, B., and Piringer, M.: Cost 715 Workshop on Urban Boundary Layer
2 Parameterizations, *Bulletin of the American Meteorological Society*, 83, 1501-1504,
3 10.1175/bams-83-10-1501, 2002.
- 4 Ryu, Y.-H., Baik, J.-J., Kwak, K.-H., Kim, S., and Moon, N.: Impacts of urban land-surface
5 forcing on ozone air quality in the Seoul metropolitan area, *Atmospheric Chemistry and
6 Physics*, 13, 2177-2194, 2013.
- 7 Salamanca, F., Krpo, A., Martilli, A., and Clappier, A.: A new building energy model coupled
8 with an urban canopy parameterization for urban climate simulations-part I. formulation,
9 verification, and sensitivity analysis of the model, *Theoretical and Applied Climatology*, 99,
10 331-344, 10.1007/s00704-009-0142-9, 2010.
- 11 Salamanca, F., Martilli, A., Tewari, M., and Chen, F.: A Study of the Urban Boundary Layer
12 Using Different Urban Parameterizations and High-Resolution Urban Canopy Parameters
13 with WRF, *Journal of Applied Meteorology and Climatology*, 50, 1107-1128,
14 10.1175/2010jamc2538.1, 2011.
- 15 Schell, B., Ackermann, I. J., Hass, H., Binkowski, F. S., and Ebel, A.: Modeling the formation
16 of secondary organic aerosol within a comprehensive air quality model system, *Journal of
17 Geophysical Research-Atmospheres*, 106, 28275-28293, 2001.
- 18 Solazzo, E., Di Sabatino, S., Aquilina, N., Dudek, A., and Britter, R.: Coupling mesoscale
19 modelling with a simple urban model: the Lisbon case study, *Boundary-layer meteorology*,
20 137, 441-457, 2010.
- 21 Solazzo, E., Bianconi, R., Pirovano, G., Matthias, V., Vautard, R., Moran, M. D., Wyat Appel,
22 K., Bessagnet, B., Brandt, J., Christensen, J. H., Chemel, C., Coll, I., Ferreira, J., Forkel, R.,
23 Francis, X. V., Grell, G., Grossi, P., Hansen, A. B., Miranda, A. I., Nopmongcol, U., Prank,
24 M., Sartelet, K. N., Schaap, M., Silver, J. D., Sokhi, R. S., Vira, J., Werhahn, J., Wolke, R.,
25 Yarwood, G., Zhang, J., Rao, S. T., and Galmarini, S.: Operational model evaluation for
26 particulate matter in Europe and North America in the context of AQMEII, *Atmospheric
27 Environment*, 53, 75-92, <http://dx.doi.org/10.1016/j.atmosenv.2012.02.045>, 2012.
- 28 Souch, C., and Grimmond, S.: Applied climatology: urban climate, *Progress in Physical
29 Geography*, 30, 270-279, 2006.
- 30 Tie, X., Madronich, S., Li, G., Ying, Z., Zhang, R., Garcia, A. R., Lee-Taylor, J., and Liu, Y.:
31 Characterizations of chemical oxidants in Mexico City: A regional chemical dynamical model
32 (WRF-Chem) study, *Atmospheric Environment*, 41, 1989-2008, 2007.
- 33 Tie, X., Geng, F., Guenther, A., Cao, J., Greenberg, J., Zhang, R., Apel, E., Li, G.,
34 Weinheimer, A., Chen, J., and Cai, C.: Megacity impacts on regional ozone formation:
35 observations and WRF-Chem modeling for the MIRAGE-Shanghai field campaign,
36 *Atmospheric Chemistry and Physics*, 13, 5655-5669, 10.5194/acp-13-5655-2013, 2013.
- 37 Trusilova, K., Fröh, B., Brienen, S., Walter, A., Masson, V., Pigeon, G., and Becker, P.:
38 Implementation of an Urban Parameterization Scheme into the Regional Climate Model
39 COSMO-CLM, *Journal of Applied Meteorology and Climatology*, 52, 2296-2311,
40 10.1175/JAMC-D-12-0209.1, 2013.
- 41 Wang, J., Feng, J., Yan, Z., Hu, Y., and Jia, G.: Nested high - resolution modeling of the
42 impact of urbanization on regional climate in three vast urban agglomerations in China,
43 *Journal of Geophysical Research: Atmospheres* 117, 10.1029/2012JD018226, 2012.

- 1 Wang, M. N., Zhang, X. Z., and Yan, X. D.: Modeling the climatic effects of urbanization in
2 the Beijing-Tianjin-Hebei metropolitan area, *Theoretical and Applied Climatology*, 113, 377-
3 385, 10.1007/s00704-012-0790-z, 2013.
- 4 Wang, X., Wu, Z., and Liang, G.: WRF/CHEM modeling of impacts of weather conditions
5 modified by urban expansion on secondary organic aerosol formation over Pearl River Delta,
6 *Particuology*, 7, 384-391, 10.1016/j.partic.2009.04.007, 2009.
- 7 Wang, X., Zhang, Y., Hu, Y., Zhou, W., Lu, K., Zhong, L., Zeng, L., Shao, M., Hu, M., and
8 Russell, A.: Process analysis and sensitivity study of regional ozone formation over the Pearl
9 River Delta, China, during the PRIDE-PRD2004 campaign using the Community Multiscale
10 Air Quality modeling system, *Atmospheric Chemistry and Physics*, 10, 4423-4437, 2010.
- 11 Wang, Z.-H., Bou-Zeid, E., and Smith, J. A.: A spatially-analytical scheme for surface
12 temperatures and conductive heat fluxes in urban canopy models, *Boundary-layer
13 meteorology*, 138, 171-193, 2011.
- 14 Wesely, M.: Parameterization of surface resistances to gaseous dry deposition in regional-
15 scale numerical models, *Atmospheric Environment (1967)*, 23, 1293-1304, 1989.
- 16 Yang, B., Zhang, Y. C., and Qian, Y.: Simulation of urban climate with high-resolution WRF
17 model: A case study in Nanjing, China, *Asia-Pacific Journal of Atmospheric Sciences*, 48,
18 227-241, 10.1007/s13143-012-0023-5, 2012.
- 19 Yang, Z., and Shiang-Yuh, W.: Understanding of the Fate of Atmospheric Pollutants Using a
20 Process Analysis Tool in a 3-D Regional Air Quality Model at a Fine Grid Scale,
21 *Atmospheric and Climate Sciences*, 3, 18-30, 10.4236/acs.2013.31004, 2013.
- 22 Yoshikado, H., and Tsuchida, M.: High levels of winter air pollution under the influence of
23 the urban heat island along the shore of Tokyo Bay, *Journal of Applied Meteorology*, 35,
24 1804-1813, 10.1175/1520-0450(1996)035<1804:hlowap>2.0.co;2, 1996.
- 25 Yu, M., Carmichael, G. R., Zhu, T., and Cheng, Y. F.: Sensitivity of predicted pollutant levels
26 to urbanization in China, *Atmospheric Environment*, 60, 544-554,
27 10.1016/j.atmosenv.2012.06.075, 2012.
- 28 Zhang, L., and He, Z.: Technical Note: An empirical algorithm estimating dry deposition
29 velocity of fine, coarse and giant particles, *Atmospheric Chemistry and Physics*, 14, 3729-
30 3737, 2014.
- 31 Zhang, N., Gao, Z. Q., Wang, X. M., and Chen, Y.: Modeling the impact of urbanization on
32 the local and regional climate in Yangtze River Delta, China, *Theoretical and Applied
33 Climatology*, 102, 331-342, 10.1007/s00704-010-0263-1, 2010.
- 34 Zhang, Q., Streets, D. G., Carmichael, G. R., He, K., Huo, H., Kannari, A., Klimont, Z., Park,
35 I., Reddy, S., and Fu, J.: Asian emissions in 2006 for the NASA INTEX-B mission,
36 *Atmospheric Chemistry and Physics*, 9, 5131-5153, 2009.

37
38
39
40
41

1 Table 1. List of acronyms used in this work

Acronyms	Description
LOCAL cells	the newly urbanized cells in each urban expansion scenario
ADJACENT cells	non-urbanized cells neighboring the LOCAL cells
ADVH	horizontal advection
ADVZ	vertical advection
ADV	the sum of horizontal and vertical advection
EMISS	emissions
DRYDEP	dry deposition
DIFF	turbulent diffusion
VMIX	the sum of dry deposition and turbulent diffusion
CONV	convection
CHEM	gas phase chemistry
CLDCHEM	cloud chemistry
AERCHEM	aerosol chemical and microphysical process
WETSCAV	wet scavenging

2

3

4

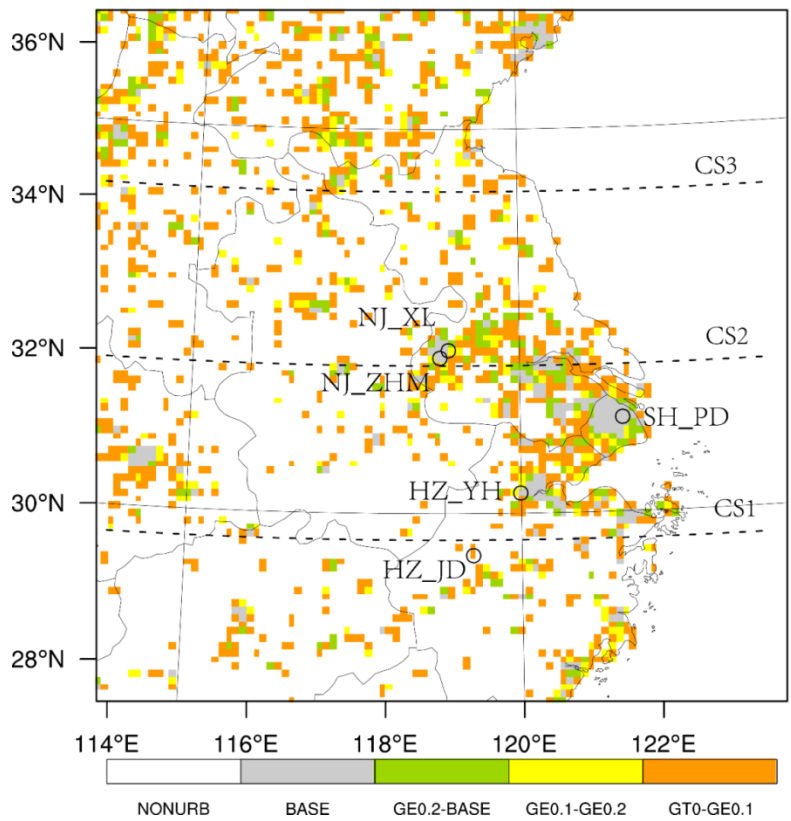
5

6

7

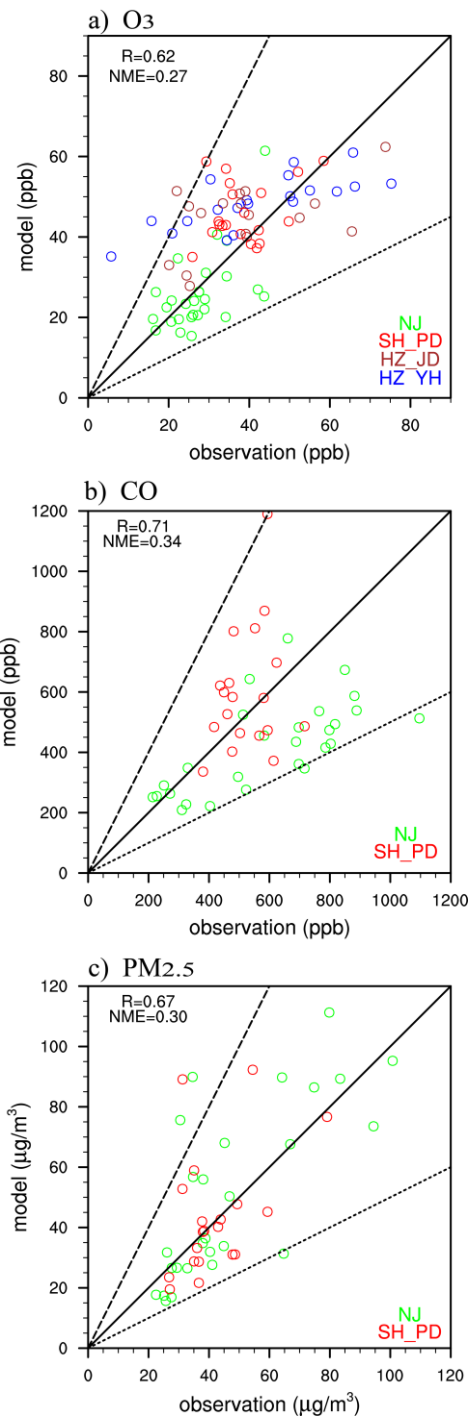
8 **Figures**

9



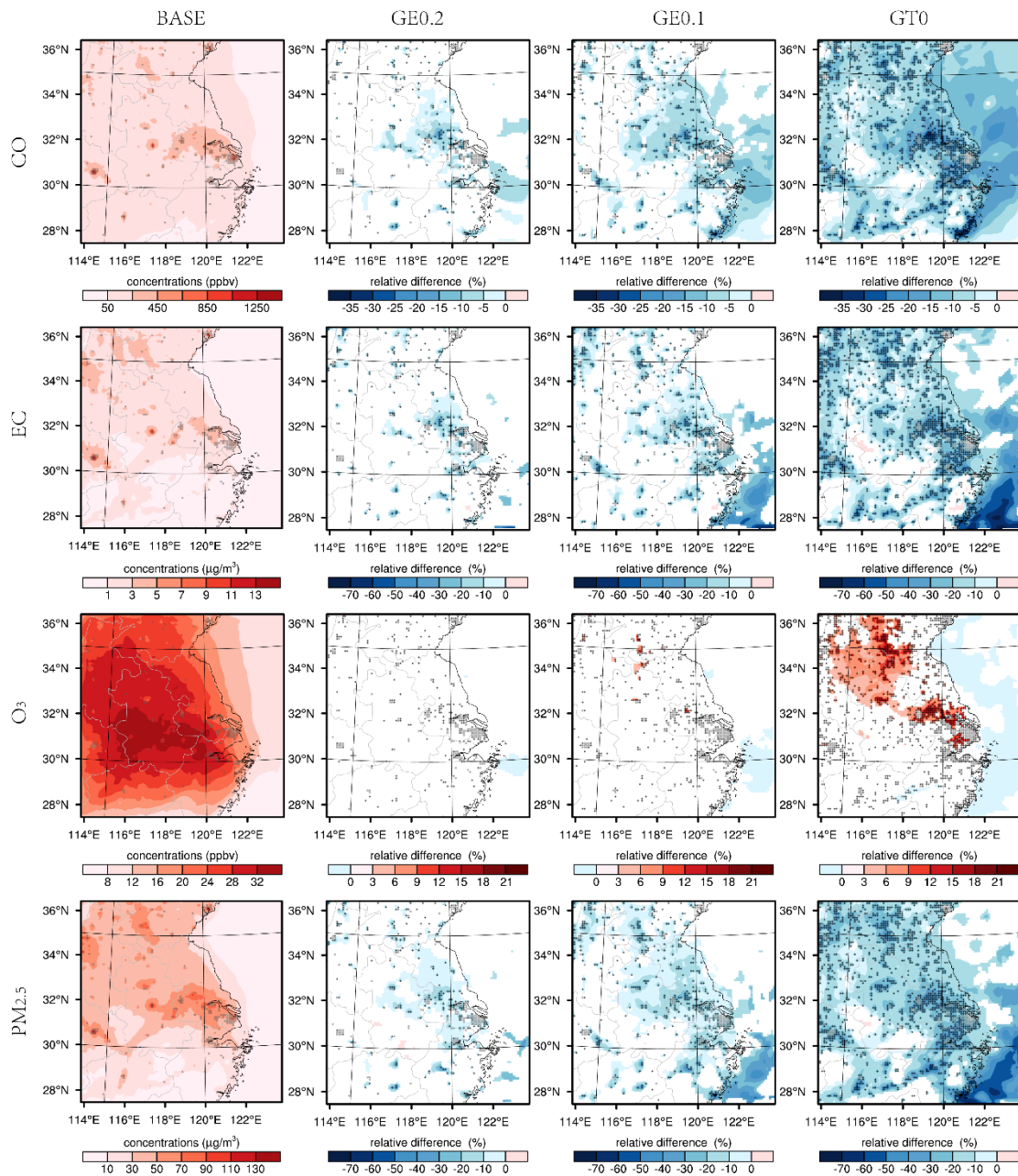
1
2
3
4
5
6
7
8
9
10
11

Figure 1. Schematic map of four idealized urban land expansion scenarios (i.e., BASE, GE0.2, GE0.1, and GT0). White denotes non-urban cells, and grey denotes urban cells in the BASE run. Other colors represent additional newly urbanized cells in GE0.2 (green), GE0.1 (yellow), and GT0 (orange) compared to previous urban land expansion scenarios. For example, urban cells in GE0.1 are grey, green, and yellow. Black open circles denote the five air quality monitoring sites. Black dashed lines running west-east demarcate the three vertical-zonal cross-sections CS1, CS2, and CS3.



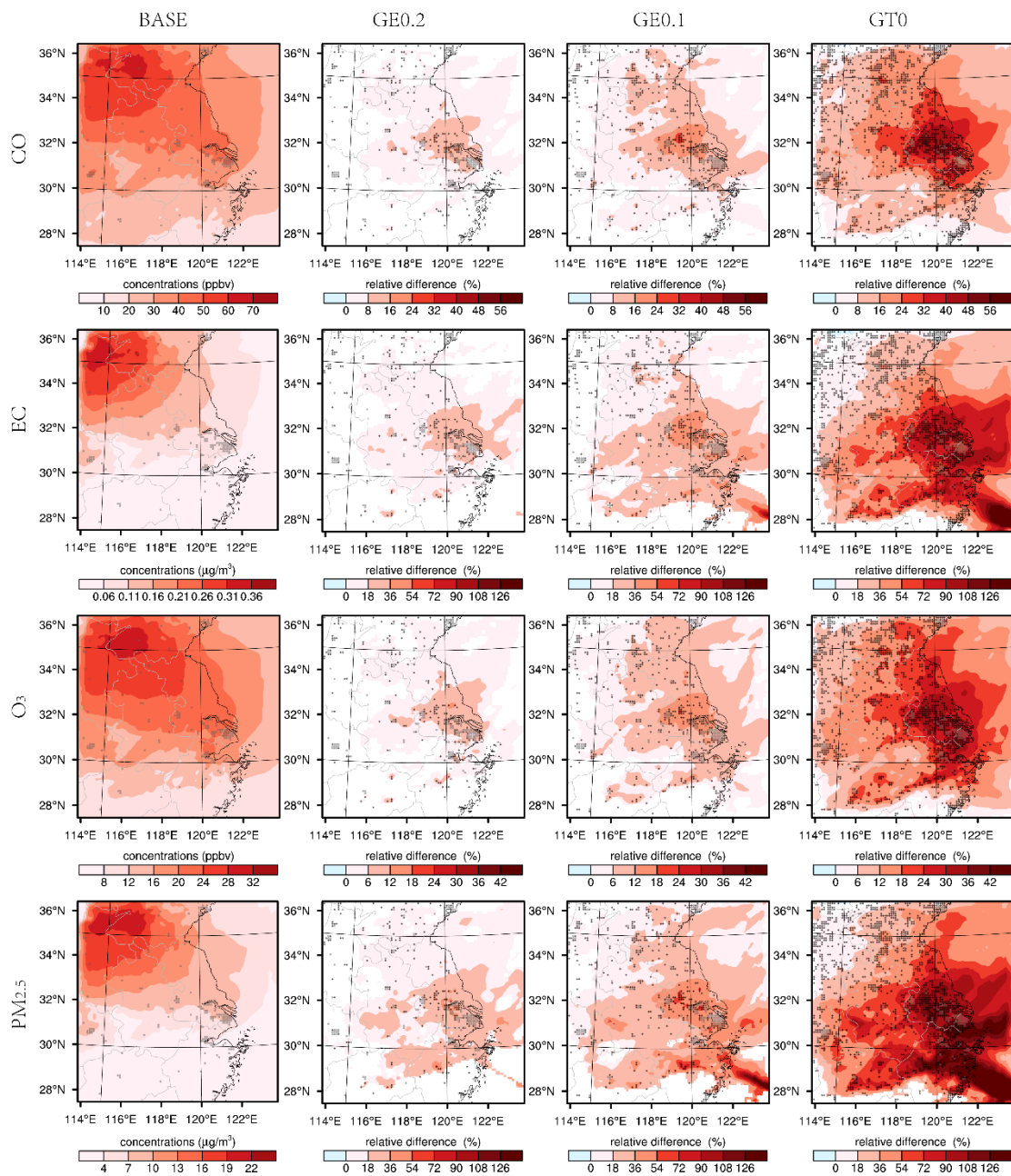
1
 2
 3
 4
 5
 6
 7

Figure 2. Modeled versus observed daily mean surface concentrations of (a) O₃, (b) CO, and (c) PM_{2.5} at NJ (07/2012), SH_PD (09/2009), HZ_YH (04/2008) and HZ_JD (04/2008). Solid line indicates the 1:1 line; dashed lines indicate the 1:2 and 2:1 lines.



1
2
3
4
5
6
7
8
9

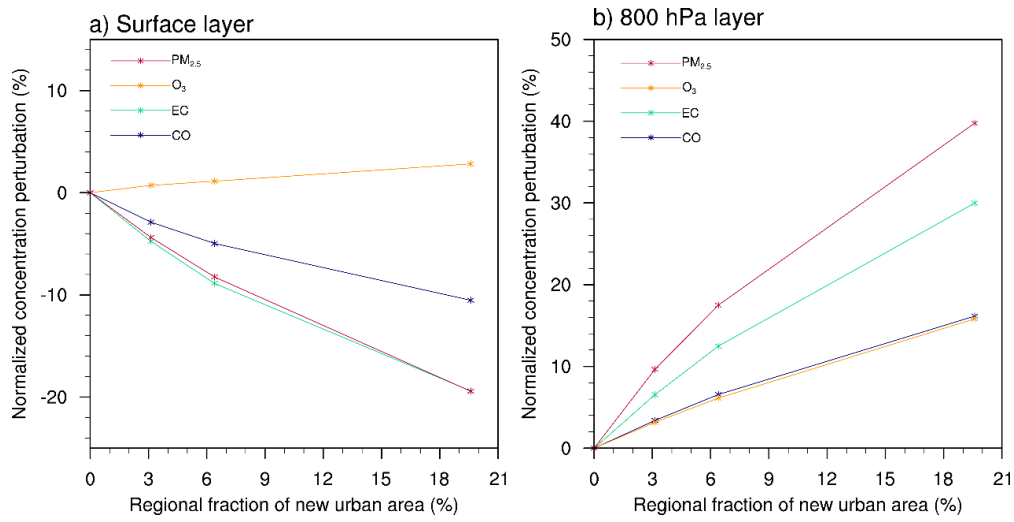
Figure 3. Five-year mean surface concentrations in July of CO, EC, O₃, and PM_{2.5} in the BASE run (left), and the relative difference (only cells exceeding the 95% significance level are shown) of each urban land expansion scenario relative to BASE (right three columns). Grey circles indicate urban areas in the BASE run; black crosses indicate newly urbanized cells in GE0.2, GE0.1, and GT0.



1
2
3
4
5
6
7
8

Figure 4. Same as Figure 3, but at 800 hPa.

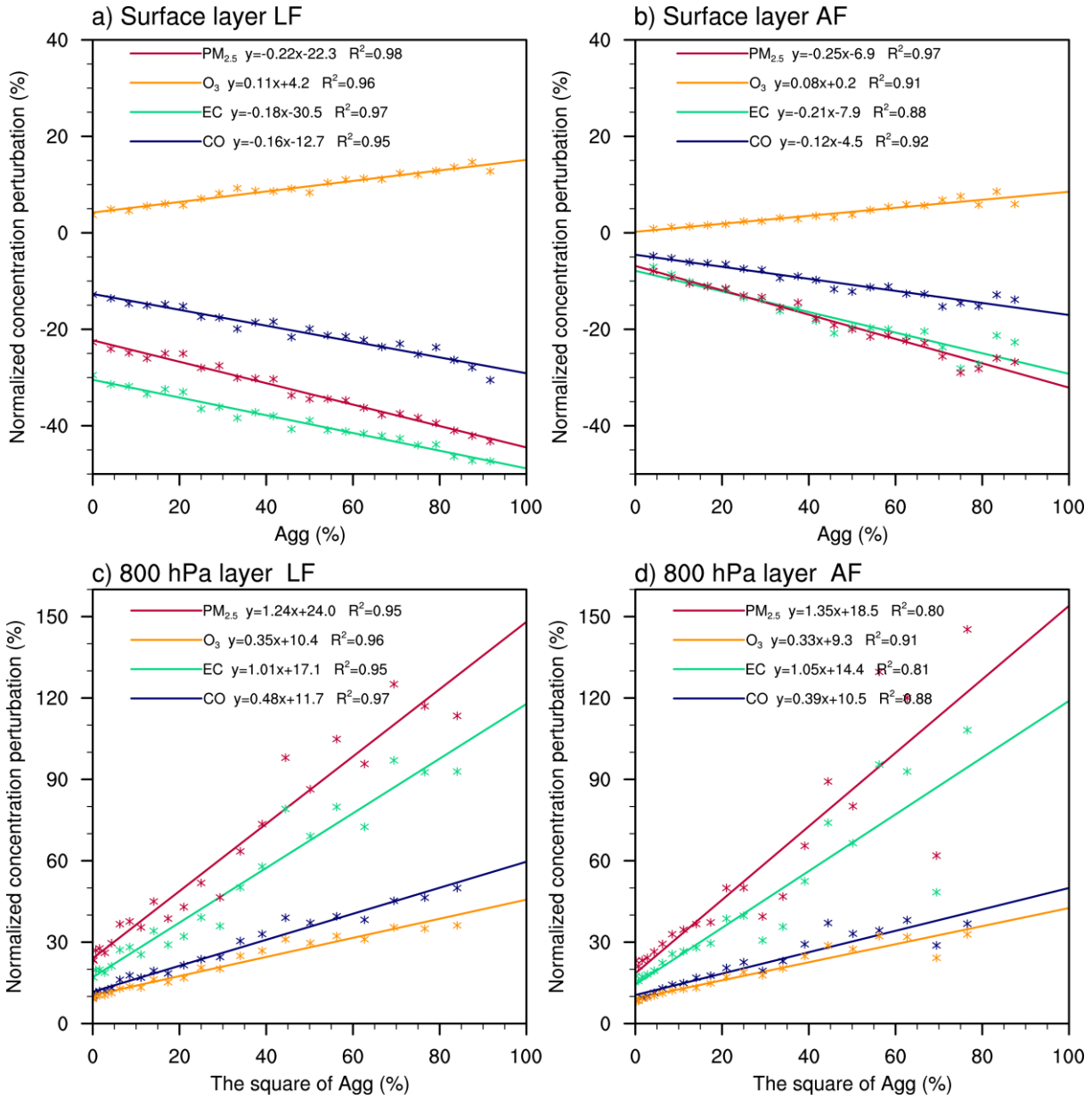
1
2
3



4
5
6
7
8
9
10
11

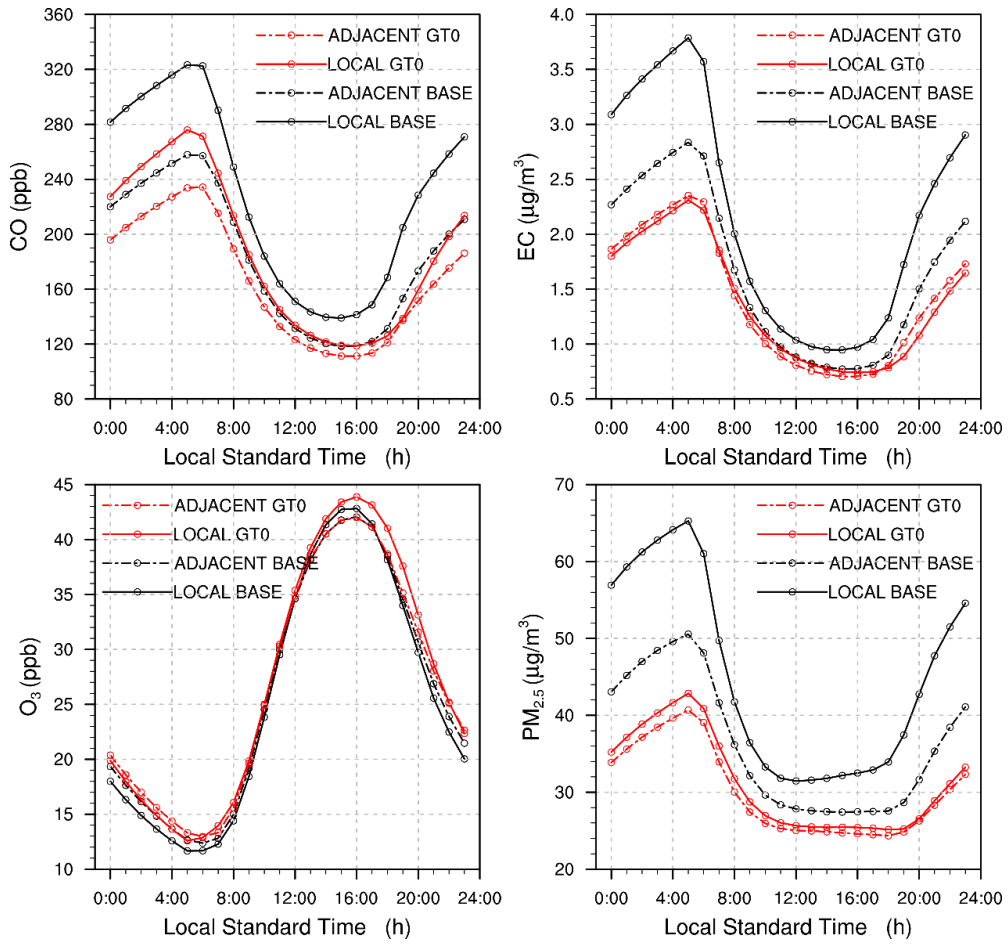
Figure 5. Normalized perturbations (relative to the BASE simulation) for three urbanization scenarios of the 5-year mean concentrations in July of CO, EC, O₃, and PM_{2.5} at the (a) surface and (b) 800 hPa. Values are averaged over land for the entire domain. Corresponding domain-wide land fraction of new urban areas are 3%, 6%, and 20%, respectively, relative to BASE.

1
2



3
4
5
6
7
8
9

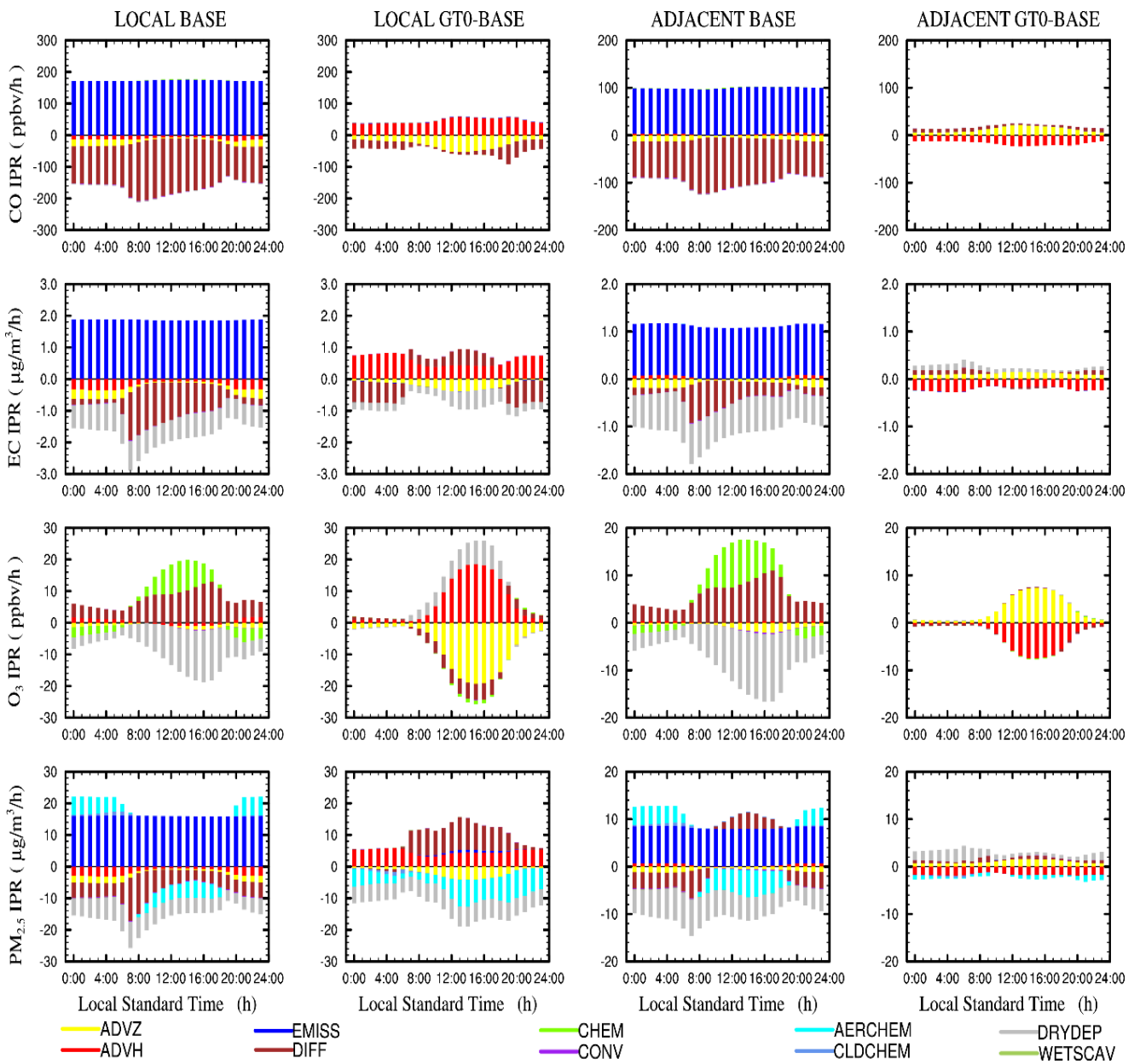
Figure 6. Relationship between normalized perturbations of 5-year mean July concentrations of CO, EC, O₃, and PM_{2.5} and Agg at the surface (top), and the square of Agg at 800 hPa (bottom) for the LOCAL forcing (LF, left) and ADJACENT forcing (AF, right). Agg is defined as the occupation rate of the newly urbanized cells to the surrounding 24 (5 × 5 - 1) cells. Linear regression results are also shown.



1

2

3 Figure 7. Simulated 5-year mean July diurnal cycle of CO, EC, O₃, and PM_{2.5} at the surface,
 4 averaged over domain-wide LOCAL cells (solid lines) and ADJACENT cells (dashed lines).

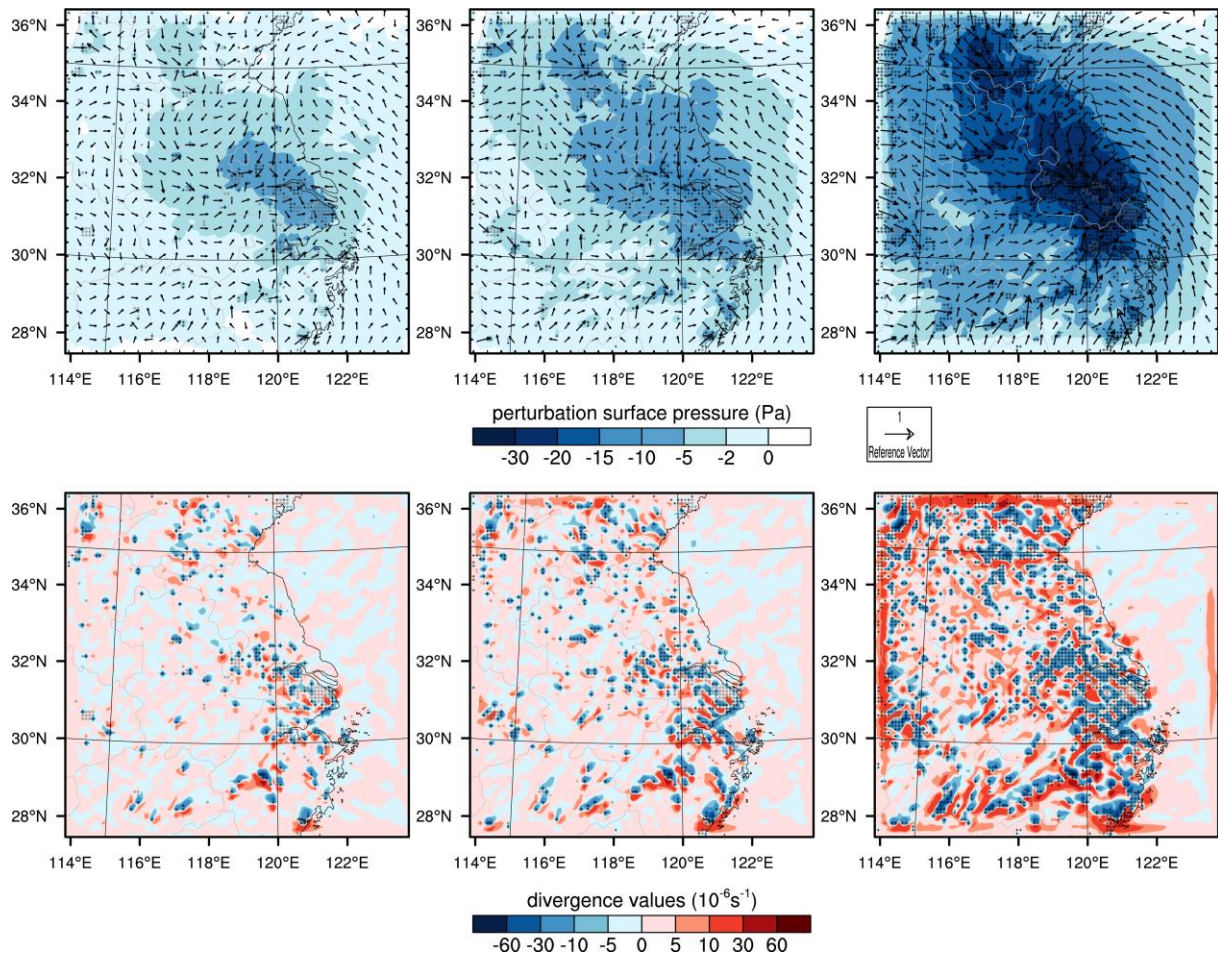


1

2

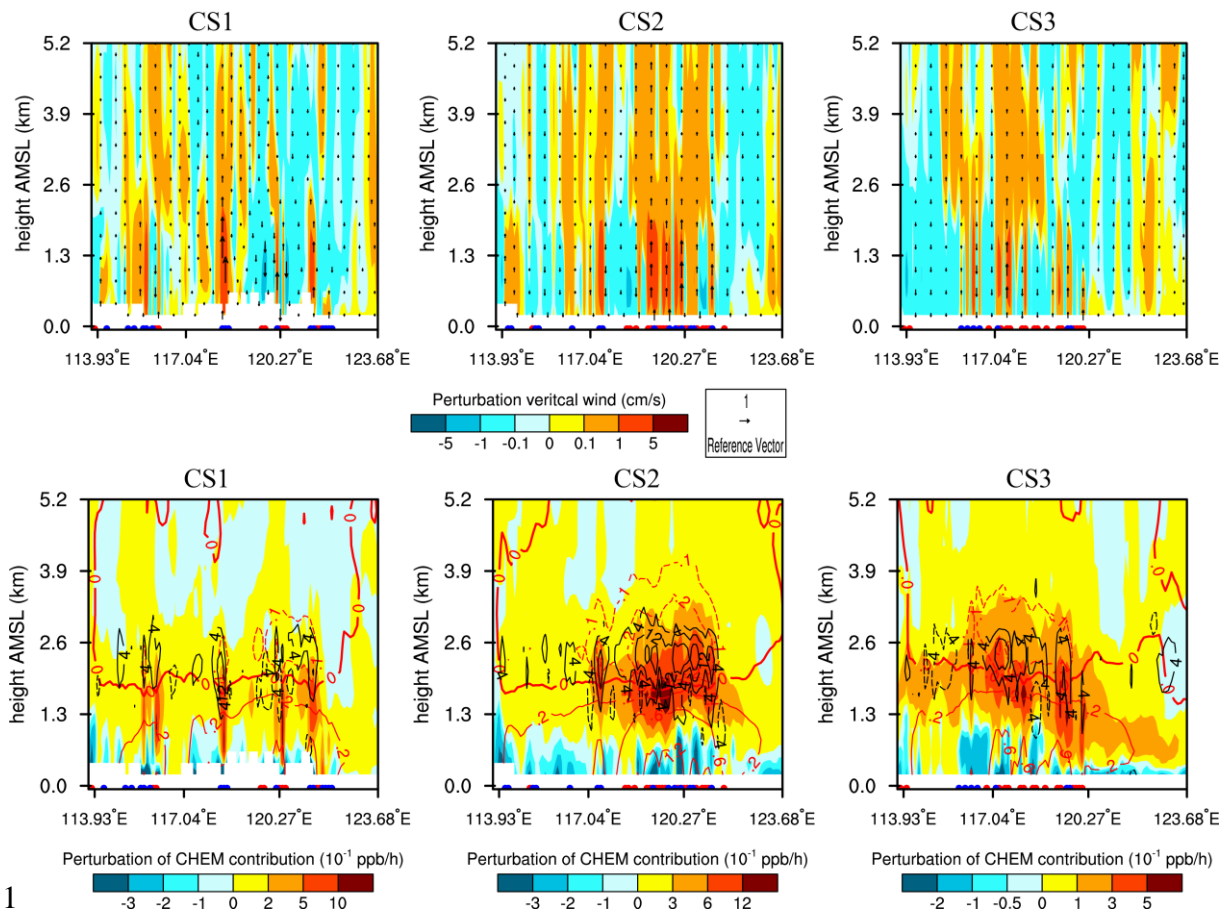
3 Figure 8. Five-year mean in July diurnal cycles of IPR for surface CO, EC, O₃, and PM_{2.5}
 4 concentrations. Values are averaged over all LOCAL (left two columns) and ADJACENT
 5 (right two columns) cells. Results are shown for the BASE simulation and for differences
 6 between GT0 and BASE.

7



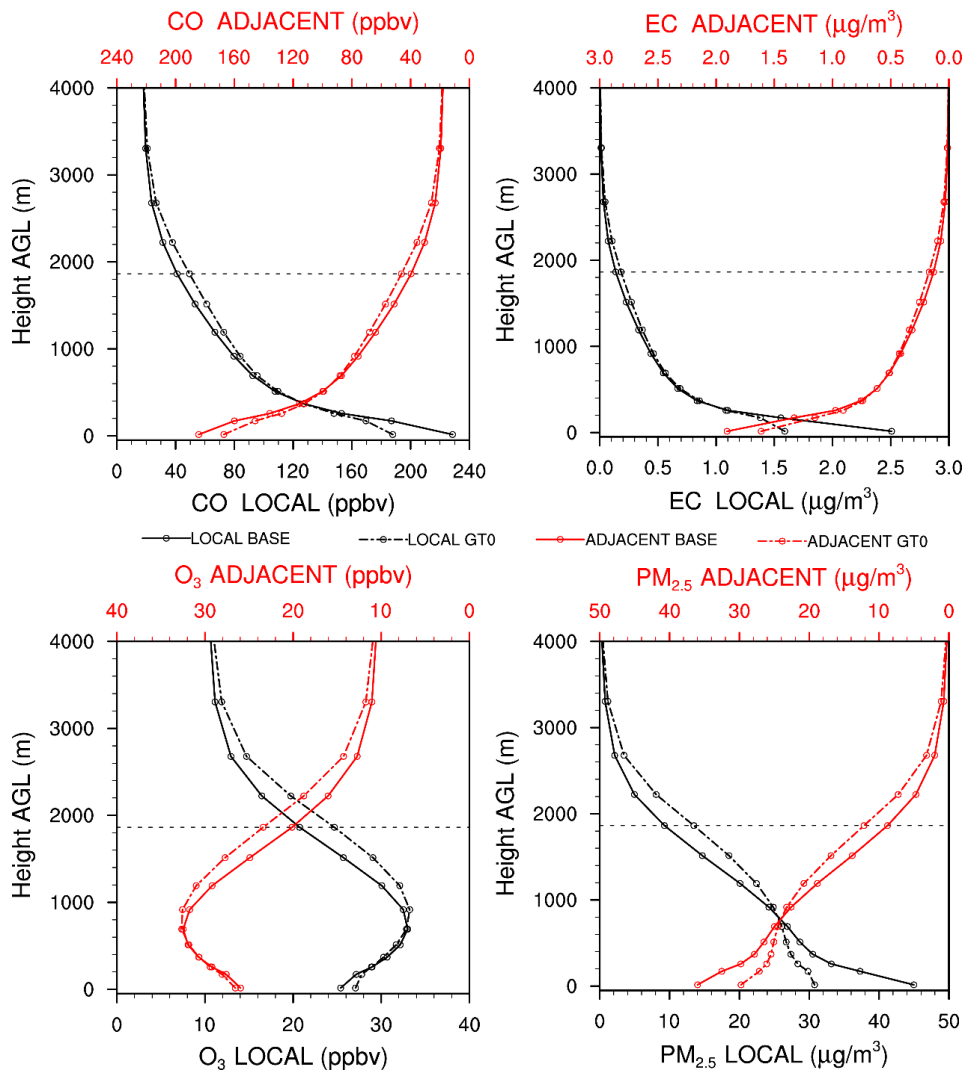
1
 2 Figure 9. Five-year mean July perturbations of surface pressure and wind field (top three plots,
 3 reference velocity is 1 m s^{-1}) and the divergence of surface wind (bottom three plots) in GE0.2,
 4 GE0.1, GT0 runs. Grey circles indicate the locations of urban cells in the BASE run; black
 5 crosses indicate the locations of newly urbanized areas in GE0.2, GE0.1, and GT0 runs.

6
 7
 8
 9



1
2

3 Figure 10. Distribution of 5-year mean July perturbations (GT0 minus BASE) of vertical wind
 4 velocities (top three plots, reference wind velocity is 1cm s⁻¹), O₃ production (color, ppb h⁻¹),
 5 cloud water content (black line, mg kg⁻¹), and air temperature (red line, K) during 12:00–
 6 17:00 LST (bottom three plots) in CS1, CS2, and CS3. Red and blue dots indicate the
 7 longitudes of LOCAL cells in the GT0 run along the cross-section lines and adjacent areas,
 8 respectively.

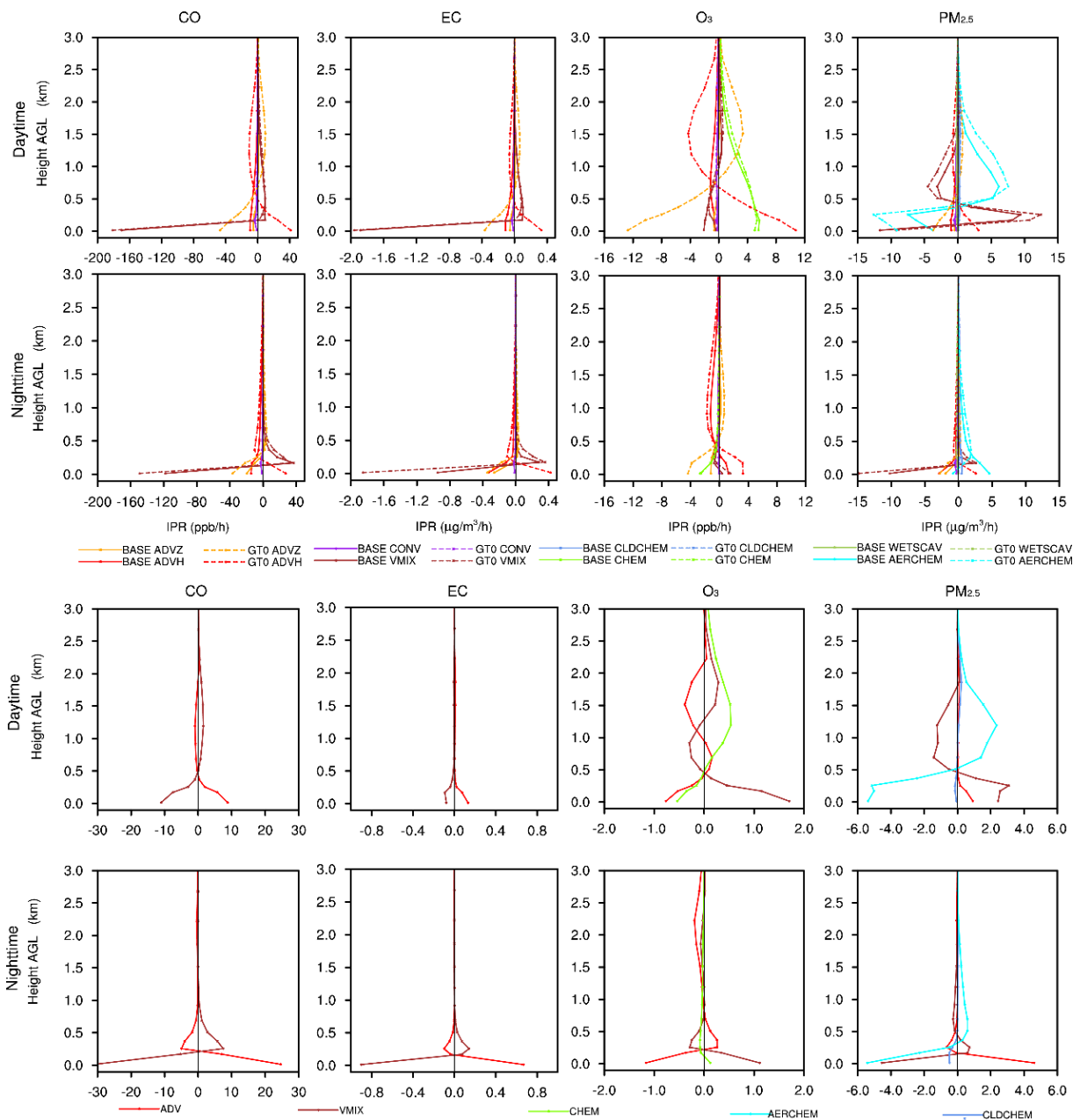


1

2 Figure 11. Five-year mean July vertical profiles of CO, EC, O₃, and PM_{2.5} concentrations over
 3 the LOCAL cells (black) and ADJACENT cells (red) in the BASE (solid lines) and GT0 run
 4 (dashed lines). The horizontal dashed lines indicate the height of 800 hPa.

5

6



1

2 Figure 12. Five-year mean in July vertical profiles of diurnal (07:00–18:00 LST) and
 3 nocturnal (19:00–06:00 LST) IPR for CO, EC, O₃, and PM_{2.5} concentrations in the BASE and
 4 GT0 run (top eight figures). The bottom eight plots show the difference in IPR between GT0
 5 and the BASE simulation averaged over domain-wide LOCAL cells.

6